# Connectome-based Predictive Models of General and Specific Cognitive Control

Shijie Qu[1,2], Yueyue Lydia Qu[1,2], Kwangsun Yoo[4,5], Marvin M. Chun[1,2,3]

[1] Department of Psychology, Yale University, New Haven, CT, USA

[2] Wu Tsai Institute, Yale University, New Haven, CT, USA

[3] Department of Neuroscience, Yale School of Medicine, New Haven, CT, USA

[4] Department of Digital Health, Samsung Advanced Institute for Health Sciences and Technology, Sungkyunkwan University, Seoul, South Korea

[5] AI Research Center, Data Science Research Institute, Samsung Medical Center, Seoul, South Korea

* Corresponding authors: Shijie Qu, Department of Psychology, Yale University, USA, or via e-mail: shijie.qu@yale.edu; Kwangsun Yoo, Department of Digital Health; Sungkyunkwan University, South Korea, or via e-mail: rayksyoo@skku.edu; Marvin M. Chun, Department of Psychology, Yale University, USA, or via e-mail: marvin.chun@yale.edu.

## Abstract

Cognitive control, the ability to adapt thoughts and actions to shifting contexts and goals, is composed primarily of three distinct yet interrelated components: Inhibition, Shifting, and Updating. While prior research has examined the nature of different cognitive components as well as their inter-relationships, fewer studies examined whole-brain connectivity to predict individual differences for the three cognitive components and associated tasks. Here, using the Connectome-based Predictive Modelling (CPM) approach and open-access data from the Human Connectome Project, we built brain network models to successfully predict individual performance differences on the Flanker task, the Dimensional Change Card Sort task, and the 2-Back task, each putatively corresponding to Inhibition, Shifting, and Updating. We focused on grayordinate fMRI data collected during the 2-Back tasks after confirming superior predictive performance over resting-state and volumetric data. High cross-task prediction accuracy as well as joint recruitment of canonical networks, such as the frontoparietal and default-mode networks, suggest the existence of a common cognitive control factor. To directly investigate the relationships among the three cognitive control components, we developed new measures to disentangle their shared and unique aspects. Our analysis confirmed that a shared control component can be well predicted from functional connectivity patterns densely located around the frontoparietal, default-mode and dorsal attention networks. In contrast, the Shifting-specific and Inhibition-specific components exhibited lower cross-prediction performance, indicating their distinct and specialized roles. Notably, the Updating-specific component showed significant cross-prediction with the general control factor, suggesting its central role in cognitive control. Given the limitation that individual behavioral measures do not purely reflect the intended cognitive constructs, our study demonstrates the need to distinguish between common and specific components of cognitive control.

## Introduction

Cognitive control, also referred to as executive functions or executive control, is the process of aligning one's cognition and behavior with current goals. Cognitive control may be categorized into three main processes (Miyake et al., 2000; Lehto et al., 2003; Diamond, 2013): Inhibition, Shifting, and Updating. Inhibition involves actively suppressing the dominant response and is assessed through tasks like the Stroop task (Stroop, 1935), the Flanker task (Eriksen & Eriksen, 1974), and the Stop Signal task (Logan & Cowan, 1984). Shifting, sometimes called cognitive flexibility, occurs when individuals switch between multiple tasks, measured through tasks like the Wisconsin Card Sorting Test (Berg, 1948), the Dimensional Change Card Sort (Frye et al., 1995), and the Color/Shape Switching tasks (Hayes et al., 1998). Lastly, Updating involves continually monitoring pertinent information and integrating it into our finite working memory, which can be measured via tasks like the N-Back task (Kirchner, 1958), the Sternberg task (Sternberg, 1966), and the backward Corsi task (Isaacs & Vargha-Khadem, 1989).

The relationship between different forms of cognitive control has been extensively studied in behavioral experiments. Using large batteries of cognitive tasks, Miyake and colleagues (2000) originally discovered that the performances of all tasks can be loaded onto the three factors: Inhibition, Shifting, and Updating. However, these three factors are intercorrelated. In an attempt to refine the model, Friedman and Miyake (2017) replaced the original Inhibition factor with a general control factor that is highly loaded by all tasks, resulting in a model with a better fit and more orthogonal factors, which they termed as the "Unity and Diversity" of executive functions (Friedman & Miyake, 2017). The different control processes are interdependent. For instance, people with superior working memory performance are also more likely to achieve a higher Inhibition score, suggesting that successful working memory may rely on actively inhibiting distractors irrelevant to one's goals (Conway et al., 2001; Mj & Rw, 2003; Unsworth et al., 2004; Kane et al., 2007). Similarly, Shifting also displays a positive relationship with working memory (Baddeley et al., 2001; Emerson & Miyake, 2003) and Inhibition (Mayr & Keele, 2000; Koch et al., 2010).

Beyond the behavioral level, researchers have long strived to uncover the neural systems underlying each cognitive control component. Earlier lesion studies indicated that damage to the prefrontal cortex may impair performance in different control tasks, but the exact anatomical locations differed across studies and the type of process targeted (Aron et al., 2003, 2004; Floden & Stuss, 2006; Barbey et al., 2013). Empirical studies and meta-analyses of fMRI data have also revealed multiple brain regions such as the lateral prefrontal cortex, posterior parietal cortex, and dorsal anterior cingulate cortex with both similar and different roles across various cognitive control components (Assem et al., 2024; Derrfuss et al., 2005; Kim et al., 2012; McNab et al., 2008; Niendam et al., 2012; Rodríguez-Nieto et al., 2022). Discrepant results across studies may lead to different conclusions being drawn about the relationship between control processes, such as the superordinate role of the Updating component (Lemire-Rodger et al., 2019; Rodríguez-

Nieto et al., 2022) or the existence of a core cognitive control network in the brain (Niendam et al., 2012).

While univariate fMRI analyses inform us about the brain regions whose activity is modulated by task conditions, connectivity-based approaches enable us to peek into the interaction between different brain regions and how they may be related to individual differences in task performance (Friedman & Robbins, 2022a; Menon & D'Esposito, 2022). In the realm of cognitive control, researchers have shown that the prefrontal cortex's global functional connectivity as well as structural connectivity profiles can predict one's cognitive control ability (Cole et al., 2012; Smolker et al., 2015). Furthermore, the performance in the three types of control tasks may correspond with different sets of functional connectivity profiles: Inhibition was highly related to the connectivity strength between the frontoparietal and cingulo-opercular networks (Deck et al., 2023); Shifting scores were correlated with the strength of connectivity within the cingulo-opercular network (Reineberg & Banich, 2016), between the default mode and the dorsal attention networks (Deck et al., 2023), and between the medial frontal and default mode networks (Chén et al., 2019). Updating performance was reflected in the frontoparietal network connectivity profiles (Reineberg & Banich, 2016), and between the angular gyrus and ventral attention network (Reineberg et al., 2015). Another insightful study found that connectivity between the cerebellum and the frontoparietal network predicts a general control factor score (Reineberg et al., 2015), but their analysis was limited to resting-state data, and the use of an ICA approach restricted their focus to highly synchronized brain regions.

In the current study, we aim to characterize the unity and diversity of cognitive control processes by relating individual differences to their brain-wide connectome profiles. To achieve this, we employed an entirely data-driven approach, the Connectome Predictive Modeling (CPM) method (Finn et al., 2015; Shen et al., 2017), to extract the relevant functional connectivity features of distinct cognitive control processes. CPM has previously shown exceptional capability in utilizing brain connectomic features to predict cognitive performance such as sustained attention (Rosenberg et al., 2016; Yoo, Rosenberg, Kwon, Lin, et al., 2022), fluid intelligence (Finn et al., 2015; Yoo et al., 2019), creativity (Beaty et al., 2018), and working memory (Avery et al., 2020). In this study, we extend the application of CPM to study the unity and diversity of the cognitive control task measures of Inhibition, Shifting, and Updating.

Both the behavioral scores and neuroimaging data used in this project were obtained from the open-access Human Connectome Project (HCP) dataset (Van Essen et al., 2012). We used their Flanker task as a measure for Inhibition, the Card Sort task for Shifting, and 2-Back tasks for Updating. For our analysis, while both resting-state and 2-Back task data were used to build CPMs, we focused our analyses on the latter due to its higher data quality (Huijbers et al., 2017), greater test-retest reliability (Kristo et al., 2014; Rosazza et al., 2014; Wang et al., 2017), and superior predictive accuracy (Greene et al., 2018, 2020; Yoo et al., 2018).

Using CPM, we explored the unity and diversity of cognitive control from two distinct perspectives. First, we developed CPM models based on the three raw cognitive control measures. By evaluating the models' within-task and cross-task predictive prediction performance, we could infer the separability and interdependence of different cognitive control components. That is, the more a model's prediction generalize from one task to another, the more they can be viewed as overlapping. Additionally, by examining the underlying connectome profiles, we assessed the differential contributions of canonical functional networks to each control component. The second approach addressed the limitation that individual behavioral measures may not purely reflect the intended cognitive constructs. We developed measures by extracting or regressing out common variance to specifically target the shared and distinct features of the three cognitive control components. We then applied CPM analyses to these refined measures to uncover their connectome foundations.

## Method

### FMRI Data

The data for this project comes from the WU-Minn Human Connectome Project (HCP) (Van Essen et al., 2012) S1200 Release of February 2017. Among the various neuroimaging modalities available in the dataset, we specifically used the 3T resting-state fMRI scans and 2-back task fMRI data. Detailed scanning parameters for all fMRI sessions are available in Van Essen et al (2012).

Our initial filtering process retained subjects who had full completion of the resting-state fMRI sessions, a set of task fMRI sessions (Working Memory, Social, and Emotion tasks; The latter two were not used in this project.) as well as the full set of out-of-scanner NIH Toolbox tasks (NIH Toolbox®; n=445 removed from this step). We discarded subjects displaying significant head motion (≥ 3mm translation, ≥3° rotation, and ≥0.15 mm mean frame-to-frame displacement), or those missing head movement parameter files for any of the resting-state or task fMRI runs (n=2 removed). Furthermore, we excluded subjects with fMRI data flagged for known defects by the HCP team (n=11 removed). Consequently, our final sample comprised n=748 (female: 418) subjects. Our sample size is comparable or even larger than that of previous CPM studies (e.g., (Avery et al., 2020; Rosenberg et al., 2016)), providing sufficient statistical power to conduct functional connectivity-based prediction.

For each included participant, two resting-state sessions were available, collected across two separate days. Each session consists of two runs (about 15 minutes each) with different phase encoding directions: left-to-right (LR) and right-to-left (RL). The N-back task data was collected over two sessions, each lasting approximately 5 minutes and using 2 different phase encoding directions, the same as in the resting sessions. The N-back task session included both 2-back and 0-back blocks. However, we only analyzed the fMRI

timeseries associated with the 2-back trials, since the 0-back trials do not significantly engage working memory (Miller et al., 2009).

To compare the robustness of fMRI data representations, we tried both the volumetric (NIFTI) and grayordinate (CIFTI) fMRI data for our analysis. Both types of resting-state fMRI data were processed using the HCP minimal preprocessing pipeline (Glasser et al., 2013). The volumetric data was registered to 2mm MNI space, while the grayordinate data was additionally transformed to the standard CIFTI grayordinate space. Further preprocessing of the volumetric data involved customized Python code to remove 12 motion parameters, white matter and cerebral spinal fluid (CSF) signals, global signals, and linear trends in the timeseries data. For the resting-state grayordinate fMRI data, we used a version further denoised by an additional ICA-FIX procedure (Salimi-Khorshidi et al., 2014), which enhances the signal-to-noise ratio by isolating and removing independent components linked to motion and other artifacts. Additionally, white matter and CSF signals, global signals, and linear trends were regressed out for consistency with the volumetric preprocessing.

The 2-back volumetric fMRI data underwent the same preprocessing procedures as the resting-state data. However, for the 2-Back grayordinate data, ICA-FIX was not applied due to insufficient data to train the denoising classifier. Instead, we regressed out the 12 motion parameters as done in the volumetric case, followed by the same nuisance variable regression for white matter and CSF, global signal, and linear trend.

**Behavioral Data**

The behavioral data for this project were derived from the performance measures for the 2-back task, the Dimensional Change Card Sort Test (DCCS), and the Flanker task from the HCP dataset. Every subject included in our neuroimaging sample had all 3 behavioral scores available. The 2-back task was conducted inside the scanner during the working memory session, whereas the DCCS and Flanker tasks were completed outside during a "NIH Toolbox Behavioral Tests" session. Both accuracy and response time were recorded for all 3 tasks and integrated into a normalized score for each subject. The scores for DCCS and Flanker were provided by the HCP team and preprocessed in accordance with the procedures detailed in the NIH Toolbox Scoring and Interpretation Guide found in the reference section. For the 2-back task, we processed the 2-back accuracy and response time for each individual following the same procedure using our customized Python code. The only modification we made was to lower the accuracy threshold from 4 to 2 when combining accuracy and threshold, to ensure data normality. All measurements were normalized to have a mean of 100 and a standard deviation of 15, following the standard normalization procedure outlined in the NIH Toolbox manual. Note that the out-of-scanner List Sorting scores were excluded as a measure of Updating since the task did not record response time data.

**Connectome-based Predictive Modelling**
Connectome-based Predictive Modelling (CPM) (Finn et al., 2015; Shen et al., 2017) links individual differences in brain functional connectivity and behavior measures.

To construct the functional connectivity matrices, we utilized the Shen268 (Shen et al., 2013) whole-brain atlas for parcellating the volumetric data, and Schaefer300 atlas (Schaefer et al., 2018) for parcellation of the cortical part of the grayordinate data. The average timeseries within each ROI was computed to represent the activity at that node, and pairwise Pearson correlation of all nodes was used to generate the functional connectivity matrix for each subject. Each Pearson r value underwent Fisher transformation to obtain a z value. For ease of calculation, we vectorized each individual's connectivity matrix and concatenated them to form the connectivity matrix for the entire sample. It is important to note that each scanning session (e.g., REST1, REST2, WM) yields two connectivity matrices corresponding to the two different phase encoding runs (L-R and R-L). Consequently, we averaged these two matrices to produce a single connectivity matrix for that session. For resting-state data, since there are two resting state sessions, we further averaged the two to obtain the final resting state functional connectivity matrix for each individual.

**CPM Prediction of Cognitive Control**
We constructed CPMs for the three cognitive control components – Inhibition, Shifting, and Updating – by using behavioral measures from the Flanker task, the Dimensional Change Card Sort (abbreviated as "Card Sort" below) task, and the 2-Back task, respectively.

The CPM approach involves two principal stages: feature selection and model fitting. During feature selection, we used Pearson's correlation to associate the connectivity edges with the behavior measure, identifying the correlation score between each edge and the selected behavior. Only edges surpassing the significance threshold ($p<0.01$, two-sided) were kept for model fitting. This process distinguishes two types of edges for selection: positively-associated edges (referred to as "positive edges" hereafter) and negatively-associated edges ("negative edges"), based on the sign of their correlation with the behavior scores. To control for variations in parcellation atlas sizes and further constrain the model to the most predictive edges, we retained only the top 100 significant positive and negative edges for subsequent analysis. Next, to fit the model, we summed together the selected positive and negative edge weights for each participant to generate an aggregate positive score and an aggregate negative score, respectively. Three linear regression models are then developed: one using the positive score only ("positive model"), one using the negative score only ("negative model"), and one combining both scores ("both model").

To evaluate predictive performance without overfitting, we employed a 10-fold cross-validation method. Specifically, we shuffled and divided the data into 10 equal parts,

training the CPM on 9 of them and testing it on the remaining one. This procedure is iterated 10 times, ensuring each fold is used for testing exactly once. The training set is utilized for feature selection and model fitting, whereas the testing set is for assessing the model's performance. Pearson's correlation between the predicted and actual behavioral scores is computed to gauge the model's prediction accuracy. The average correlation across all 10 folds serves as the final measure of model fit. This process was repeated 1,000 times, with a different shuffle each time, to confirm the reliability and reproducibility of our findings. The mean model fit score across these 1,000 iterations was reported as the model's final score. Additionally, a permutation test follows the same steps but with the subject's behavioral scores randomly shuffled before being split into folds, ensuring a rigorous evaluation of model performance.

We assessed the within-task prediction accuracy of each CPM – evaluating the prediction for the same task on which the model was trained. This approach allows us to directly ascertain whether the individual differences in functional connectivity identified by the CPM model are robust enough to accurately predict new data.

In addition, we explored cross-prediction across every pair of tasks to evaluate the generalizability of each task-specific CPM model to predict individual differences in a different task. Cross-predictions also allow us to infer the separability of different cognitive control components, namely what's common and what's specific across tasks. To this end, we tested the model on a different measure from what it was being trained on. For cross-validation, during each iteration, we maintained the exact same train-test split and applied the previously trained CPM model to predict a different task measure within the testing cohort.

**CPM Canonical Network Analysis**

We also examined the anatomy of the features selected across all models to evaluate the influence of specific anatomical/functional networks on the three cognitive measures. Due to the variability in edge selection across iterations of CPM training resulting from different training-testing splits, we included an edge only if it was selected in more than half of the total iterations (over 500 out of 1000 iterations). This approach helps preserve only core edges that reflect meaningful individual differences in behavior. To confirm that the choice of threshold did not qualitatively change the results, we varied the thresholds between 40%-60%, but did not see substantial changes of the edges within or between canonical networks.

To define canonical networks on volumetric data, we used the 10-network version of the Shen 268 atlas, where each parcel is categorized into one of the medial frontal, frontoparietal, default mode, motor, visual A, visual B, visual association, salience, subcortical, cerebellum networks. For grayordinate data, we employed the 7-network version of the Schaefer 300 atlas for cortical regions. For subcortical structures, we divided them into two separate networks based on their original label given by the CIFTI

file: a subcortical network and a cerebellum/brainstem network. Furthermore, since the subcortical network includes regions such as the hippocampus and thalamus, which are traditionally classified within the limbic network, we combined these regions with the limbic network as defined in the Schaefer 300 atlas and retained the designation "subcortical network" for consistency.

**CPM Computational Lesion Analysis**

To further assess a canonical network's contribution and importance to prediction performance, we performed a computational lesion analysis (also known as an ablation analysis). In this approach, we removed all connectivity patterns associated with a specific network and evaluated how this affected the predictive performance of CPM. Specifically, for each target network under investigation, we retrieved the CPM model trained using the standard procedure, removed all within and cross-connectivity edges associated with the target network, and then predicted outcomes on the hold-out testing set using the same cross-validation procedure.

**General and Specific Cognitive Control Analysis**

We conducted additional analyses to address the following two questions. First, is there an overarching functional connectome for general cognitive control (Unity; Friedman & Miyake, 2017)? Second, given that the original measures may not purely reflect the underlying cognitive control constructs (as indicated by their high correlation), can we identify the functional connectome unique to each construct (Diversity; Friedman & Miyake, 2017)?

To address these questions, we devised two types of measures: a general cognitive control score and three component-specific scores of Inhibition, Shifting, and Updating. The general cognitive control score was derived from the mean of the original z-scored task measures, where we hope to retain only the core information shared by different cognitive control components. On the other hand, the component-specific scores were defined as the residuals after regressing out the other two measures from each target measure, with the aim to preserve only the variance that cannot explained by other measures. We created CPMs for the general cognitive control score and the three component-specific scores.

## Results

### Different Cognitive Control Measures Are Correlated

To investigate the cognitive control components of response inhibition, set switching, and working memory updates, we used behaviors from the Flanker task, the Card Sorting task, and the 2-Back tasks, respectively.

Descriptive statistics revealed that every pair of measurements were correlated with each other (with $p<0.001$), as indicated in Table 1. The highest correlation was found between the Card Sort and Flanker measures. More statistics for each measurement can be found in Supplementary Table 1.

### CPMs Predict Individual Differences for 3 Cognitive Control Components

Table 2 shows the results of CPMs trained and tested on Flanker, Card Sort, and 2-back task data using connectomes measured during resting state (left column) or 2-back task scans (right column). Most predictions were statistically significant (Permutation test $p<0.05$, corrected for FWE). The three rows of tables correspond to CPMs based on positive, negative or both types of edges. For instance, the top left entry (0.1443) in the first sub-table corresponds to the predictive performance of a positive CPM model, when trained and tested both on Flanker measures and resting-state fMRI data.
Within-task predictions, as represented by the diagonal of each table, were significant in all cases. Notably, 2-Back was predicted significantly more accurately than Flanker and Card Sort performance ($p$'s < 0.05). More interestingly, cross-task prediction performance (that is, train the CPM on one measure and test on a different measure) was also significant in most cases (permutation test $p<0.05$, corrected for FWE). 2-Back performance was most strongly predicted when trained on any of the task measures (blue and green shading). On the other hand, cross-prediction performance for Card Sort and Flanker (both ways) was numerically lower and even non-significant when using resting-state fMRI data. This low cross-prediction score stands in stark contrast with their high correlation in behavioral measures.

Comparing the left and right columns shows that CPM performance was significantly higher from 2-Back task fMRI data than from resting-state data (p's <0.001in all cases, corrected for FWE). In other words, the 2-Back task fMRI data enabled higher prediction $r$ (permutation test $p<0.05$, corrected for FWE) across all model types and behavioral combinations.

We also examined the impact of fMRI data format on CPM performance by comparing models trained and tested on grayordinate data versus volumetric data. Grayordinate-based data showed superior CPM predictive performance over traditional volumetric-based data in most cases ($p<0.001$ in all cases using 2-back fMRI data; $p<0.001$ in 18 out of

27 cases using resting-state fMRI data, both corrected for FWE). Detailed CPM performance on volumetric fMRI data is presented in Supplementary Table 4.

Therefore, due to the greater variance captured by using grayordinate-based task fMRI data, we will primarily present the results based on 2-Back grayordinate fMRI data in the following sections. For those interested in the results on resting-state or volumetric data, which produced comparable patterns of results, please refer to the supplementary tables for further details.

**The FPN, DMN, and DAN are involved across all cognitive control components**

We next investigated the connectome anatomy for each of the cognitive control components. The resulting connectome profile for each component is depicted in Figure 1. In summary, positive predictive edges for the Flanker task were mainly within the frontoparietal network and with the dorsal attention network and cerebellum. Positive predictive edges for the Card Sort task involved mainly the frontoparietal, default mode, and salience networks. Lastly, positive predictive edges for 2-Back performance were mostly within the frontoparietal network, as well as between the frontoparietal network and both the default mode and dorsal attention networks. Overall, the edges that positively predicted the three cognitive control measures span a wide range of canonical networks and are relatively distinct from one another. The core cluster of positive edges common to all three cognitive control CPMs, illustrated in Figure 1 **(bottom right)**, was located within the frontoparietal, and between the frontoparietal, dorsal attention, and default mode networks.

On the other hand, CPM also picked up a set of negative edges that inversely relates to performance in each cognitive control task. For the Flanker task, negative edges were found within and between the frontoparietal, default mode, and dorsal attention networks, as well as some edges within the visual network. The CPM for the Card Sort task included negative edges within the default mode, visual, and salience networks, as well as between the salience network and the dorsal attention and frontoparietal networks. The negative CPM model for the 2-back task included mostly edges associated with the frontoparietal network, along with the those between the visual network and cerebellum. The intersection plot (Figure 1, bottom right) reveals that most of the negative edges common to all three CPMs were within frontoparietal and default mode networks, as well as between somatomotor and default mode networks.

**Lesioning the FPN and DMN led to largest performance drop**

To directly study the contribution of each network in predicting individual differences, we then performed computational lesion analysis on CPM by lesioning each network's connectivity one at a time. As shown in Figure 2, in the positive models, lesioning frontoparietal connectivity resulted in the largest prediction performance drop in most cases, where lesioning the default mode network showed the largest prediction

performance drop in the other cases. In the negative models, most impairments can be attributed to lesioning the frontoparietal network and especially the default mode network. To a lesser extent, lesioning other networks such as the salience and visual networks resulted in a significant drop in prediction performance.

**General Control is Predicted Better Than Specific Control**

To study the shared connectome underlying general cognitive control, as well as the idiosyncratic connectomes for specific cognitive control components, we repeated the CPM procedure on four newly devised measures: one general control score and three component-specific scores. The general cognitive control score was derived from the mean of the original z-scored task measures, and the component-specific scores were defined as the residuals after regressing out the other two measures from each target measure. More statistics for each measurement can be found in Supplementary Tables 2 and 3.

As illustrated in Table 3, when tested on the same measure as the CPM was trained on, the general control measure was predicted better than the component-specific measures using 2-back fMRI data. Also, after regressing out other non-target measures, the cross-task prediction performance between different component-specific measures was dampened.

Aligned with our earlier analysis, using 2-Back fMRI data enhanced predictive performance over the resting-state data. Therefore, the following sections will emphasize results obtained from task-based fMRI data over resting-state fMRI data. We encourage interested readers to check out the supplementary tables and figures for results in other conditions.

**The Component-specific Measures Bear Little Network Connectivity Overlap**

Examining the canonical functional networks for each component-specific positive CPM model reveals little overlap Figure 2 (bottom right), suggesting that the connectome for each cognitive control component became more unique when shared variance was removed.

While the connectome for each component looks roughly similar to the previous ones, one can spot some differences relative to the models without shared variance removed (Figure 1). For positive networks, the Flanker model now consists of fewer frontoparietal-related edges, both in terms of within frontoparietal edges and between frontoparietal and other networks such as dorsal attention network and brainstem/cerebellum. Within-salience network connectivity was more relevant to predict individual differences in performance (all $p<0.001$, FWE corrected). Similar patterns were observed for the Card Sort model, where the frontoparietal network showed fewer connections within itself and with the dorsal attention network, while the salience network's connections were increased ($p<0.001$, FWE corrected). Lastly, the 2-Back model showed fewer positive edges between

dorsal attention and frontoparietal networks, but more edges between within dorsal attention and between dorsal attention and default mode networks ($p<0.001$, FWE corrected).

Negative CPM models in Figure 3 also showed a decrease in overlapping edges relative to the models without shared variance removed (Figure 1). Again, subtle changes can be observed when closely examining each component CPM. For the Flanker task model, the reduction in within-frontoparietal edges was accompanied by an increase in the interconnection between the salience and default mode networks ($p<0.001$, FWE corrected). The Card Sort model showed more within-frontoparietal and brainstem/cerebellum-frontoparietal edges ($p<0.001$, FWE corrected). Additionally, the 2-back model showed an increase in visual-frontoparietal edges ($p<0.001$, FWE corrected).

**General Control Involves the Interplay of the FPN, DMN, and DAN**

Lastly, we examined the connectome for the general cognitive control measure, defined as shared variance across the Flanker, Card Sort, and 2-Back tasks. As shown in Figure 4, the positive edges were densely located around the frontoparietal networks, including within-network connections and its interconnections with the dorsal attention and default mode networks. Other edges, though less densely populated, mostly bridged the default mode network with other networks. In contrast, the negative edges were most numerous within the frontoparietal network, between the frontoparietal and default mode networks, and between the cerebellum and visual networks. Additionally, the dorsal attention and visual networks comprised a substantial number of inter-network connections that inversely contributed to individual behavioral differences. These findings closely align with the intersection plot in Figure 1, reinforcing its validity as the connectome for general cognitive control.

## Discussion

In this study, we provided a novel demonstration of the neural connectome profiles underlying the cognitive control components of Inhibition, Shifting, and Updating (Friedman & Miyake, 2017). Utilizing Connectome-based Predictive Modeling (CPM) to develop models trained and tested on the Flanker task for Inhibition, the Card Sort task for Shifting, and 2-Back tasks for Updating, we revealed that distributed functional connectivity patterns serve as robust predictors of individual differences in each cognitive control process in the HCP dataset. Additionally, by comparing within-task and across-task model predictions, and by averaging or regressing out different measures, we were able to investigate the shared and specific connectomes associated with the three cognitive control constructs. Our analyses further confirmed that 2-Back task and grayordinate fMRI data supported superior predictive performance over resting-state and volumetric data.

**Cross-predictions**

CPM cross-prediction patterns revealed that the 2-back (Updating) task CPM generalizes best to predict the performance in the other two tasks. The high cross-prediction performance of models trained on 2-back task suggests the central role of Updating in cognitive control, a notion supported by various prior studies. In Lemire-Rodger et al. (2019), multivariate analysis on fMRI data alluded to Updating as a common factor supporting the other cognitive control processes. In another meta-analysis, Rodríguez-Nieto et al (2022). reported that the Updating network highly overlaps with the Shifting and Inhibition networks, while the latter two exhibited minimal overlap. At the behavioral level, Updating stood out as the sole process among the three control mechanisms showing a substantial correlation with general intelligence (Friedman et al., 2006), suggesting it is domain-general. Updating, commonly operationalized as working memory, involves controlling attention to resist interference, a key component that scaffolds many higher-order executive processes (Engle, 2002; Engle et al., 1999; Kane & Engle, 2003; Unsworth et al., 2004). Our findings are less consistent with some previous studies that posited Shifting (Dajani & Uddin, 2015) and Inhibition (Miyake & Friedman, 2012) as the common components for general cognitive control.

On the other hand, the Flanker task CPM (Inhibition) and the Card Sort task CPM (Shifting) exhibited lower generalizability when applied to predict other tasks, suggesting they are distinct components in cognitive control. This proposition aligns with several previous studies (Lemire-Rodger et al., 2019; Miyake et al., 2000; Rodríguez-Nieto et al., 2022). Upon closer examination of our results using task fMRI data, we found that models trained on the Card Sort task and tested on the Flanker task performed better than those trained and tested in the opposite direction. This observation may be related to the idea that task switching is facilitated by inhibition, as smoothly transitioning to a new task set requires effectively suppressing the previous set of rules. (Davidson et al., 2006; Diamond, 2013; Koch et al., 2010).

**General and Specific Control Connectomes**

The significant CPM cross-task prediction scores indicate the presence of a general control factor that supports the three control components. This is further supported by the high CPM prediction accuracy of our general cognitive control measure, derived from the mean of the three original measures that correlated significantly with each other. The above-chance within-task prediction accuracy of the 2-Back specific CPM model, along with its high cross-predictive performance on the general control factor, emphasizes the central role of Updating in cognitive control. Conversely, the cross-prediction accuracy between flanker and card sort-specific measures were numerically lower, suggesting that they became more distinctive after removing the general aspect of cognitive control. Overall, the identification of a general control factor aligns with Miyake's theory (Miyake et al., 2000) that posited a construct that unifies different types of control processes.

Examining the functional networks supporting general executive control, we observed that many positive edges (i.e., edges that positively correlate with performance) reside in and between the frontoparietal (FPN), dorsal attention (DAN), default mode (DMN), and salience networks (SN). All of these canonical functional networks have previously been implicated in various aspects of executive control (Friedman & Robbins, 2022b; Menon & D'Esposito, 2022). The FPN is associated with the initialization and adjustment of control, executive task performance and interactions between attention and other cognitive processes (Dosenbach et al., 2008; Marek & Dosenbach, 2018; Seeley et al., 2007). The DAN directs top-down attention and assists successful spatial attention (Corbetta & Shulman, 2002, 2011; He et al., 2007). The SN plays a role in perceiving event saliency, monitoring conflicts, and initiating access to working memory and attention (Carter & van Veen, 2007; Menon & Uddin, 2010). Finally, although the DMN tends to quench its activity during tasks, it has a putative role in switching between internal and external attention modes (Leech et al., 2011). Additionally, we also found a number of positive edges in the visual network (VN). Although this may not be directly related to cognitive control, the strength of connectivity within the VN is consistent with the fact that all three tasks involved visual perception (Baldassarre et al., 2012).

While each of these networks serve their distinct roles in executive control, they communicate with each other to subserve more complicated control processes, as reported by various prior studies. For instance, researchers have found that the FPN shows differential connectivity patterns with the DMN and the DAN. The former strengthens during cue-independent introspective tasks, while the latter relates more to perceptual attention (Dixon et al., 2018). Another study revealed that the connectivity between the DMN and other task-related networks (e.g., the SN, FPN) were strengthened during a battery of tasks and is correlated with task performances (Elton & Gao, 2015). Aligned with these results, our general control CPM picked up these connectivity features, and thus further consolidate the notion that these functional networks may act as hubs for general cognitive control.

Interestingly, some connectivity features that negatively correlated with general control performance were from the same set of canonical networks. For instance, a high proportion of edges within the FPN and between the FPN and DMN appeared in both the positive and negative models. One possible interpretation is that the canonical networks such as FPN encompasses a large number of brain regions that may be heterogeneous in their contributions to cognitive control (cf. Dixon et al., 2018). As a result, the connectivity strength of different subregions may correlate differently with performance measures.

While many of the identified edges have established roles in prior studies, CPM also detected numerous edges that are less reported. For instance, our results revealed an inverse relationship between general control performance and the cerebellum's co-activation with the VN. However, we did not find much reported about the cerebellum's negative correlation on cognitive performance. Therefore, confirming or disproving this relationship warrants deliberate investigation in the future. Overall, we believe that CPM

can play a valuable role in expanding our current knowledge base by generating new hypotheses for future testing.

We also explored whether the neural basis of general control overlaps with that of attention, a well-studied cognitive process, at the connectome level. To investigate this, we conducted a separate analysis using an externally validated connectome model of general attention from Yoo et al. (2002) to predict general control performance here. The cross-prediction accuracy on general control was significant but numerically much lower than when predicted using general control CPM (Supplementary Table 9a), suggesting that general control is distinct from the general attention mechanism. When applied to the three original cognitive control measures, the general attention CPM showed numerically lower prediction accuracy than the general control CPM (Supplementary Table 9b), reinforcing the idea that attention does not fully account for cognitive control. Note that for consistency with the general attention connectome predictive modeling (CPM) specifications, we utilized resting-state volumetric fMRI data for this comparison across studies.

On the other hand, the connectome profiles for each component-specific measure were more distinct from one another. For example, in the positive models, the Flanker task was characterized by a high density of edges within the FPN, DMN, and SN. In contrast, the Card Sort task showed more edges connecting the DMN with the SN and DAN. The 2-Back task's edges were primarily concentrated within and between the FPN, DMN, and DAN. These network motifs might hint at unique signatures for each specific control component.

**FMRI Data Representations**

Throughout our analysis, we also studied the impact of fMRI data representation and brain state on CPM performance. We found that using grayordinate (CIFTI) data provides significant boost in CPM predictive accuracy over traditionally used volumetric (NIFTI) data. This advantage can be attributed to the inherent benefit of using grayordinate data, which registers the cortical areas into a flat surface, while maintaining 3D structures of subcortical areas. By doing so, it provides a more compact representation with higher inter-subject spatial correspondence (Glasser et al., 2013), better signal-to-noise ratio (Smith et al., 2013), and reduced signal contamination that inflates functional connectivity (Brodoehl et al., 2020). Admittedly, this is not an exhaustive comparison between the two data representations, but it suggests that a well-chosen fMRI data format can enhance CPM analysis performance. More dedicated comparisons in the future may provide deeper insights into the best practices for CPM analysis.

**Brain States**

Comparing between resting state data with 2-Back task-based fMRI data, we noticed a significant improvement associated with the use of 2-Back data across both volumetric and gradyordinate data representation formats. This enhancement is consistent with

previous findings that task-based fMRI data generally aids in more accurate prediction of traits and behaviors, even if the task data differs from the behavior being predicted (Elliott et al., 2019; Finn & Bandettini, 2021; Greene et al., 2018; Jiang et al., 2020; Yoo et al., 2018; Yoo, Rosenberg, Kwon, Scheinost, et al., 2022). In combination with other reported benefits of task fMRI data, such as its greater information gain for inferring hidden parameters (Tuominen et al., 2023), less head motion during acquisition (Huijbers et al., 2017), and better test-retest reliability for network identification (Kristo et al., 2014; Rosazza et al., 2014; Wang et al., 2017), when possible, we support the use of task-based fMRI data over resting-state data (or a hybrid use of resting and task, see Finn, 2021 for further perspectives) to achieve better predictive accuracy.

**Limitations**

While our study provides a fresh perspective on the connectome profiles of various control processes, we also consider several limitations of our current approach as well as potential future directions. First off, the so-called task impurity problem (Burgess, 1997; Phillips, 1997) poses a serious challenge to accurately measuring the psychological processes targeted by executive function tasks. Because each cognitive control task typically involves a combination of cognitive, perceptual, and motor processes, it becomes nearly impossible to assert that the variance captured by the model reflects only the intended process. Given the inherent difficulty in creating a "pure" executive control task, our project takes the valuable approach of distinguishing between the common and specific components that each cognitive control score measures. Future work could build on these analyses by extending it to other cognitive and non-cognitive measures, allowing us to evaluate the extent to which each task relies on general versus specific control components, as well as the generalizability of our cognitive control connectome.

Secondly, due to the constrained nature of public neuroimaging datasets, we were only able to build our CPMs on the 2-Back and resting-state data. While the 2-Back data already demonstrates good predictive performance across all three behavior measures, it would be valuable to replicate these analyses using other types of cognitive control-related task fMRI data. A similar concern is that the connectome profile captured using 2-Back fMRI data differs from that obtained using resting-state data. Interpreting this discrepancy is essential to developing a connectome profile of cognitive control that is agnostic to brain state.

An additional limitation is that our CPM network analysis is based on canonical functional networks, which are suitable for prediction but may be coarse for detailed examination of connectome features. As noted above, each canonical network (e.g., the FPN) may be functionally heterogeneous. The next step could focus on developing novel, optimized methods to achieve more fine-grained delineations of the canonical networks, leading to clearer explanations of each network's functional contributions.

Another limitation is that our study was focused on healthy adults. As previously revealed cognitive control and prefrontal cortex undergo prolonged developmental trajectories before stabilizing in adulthood (Anderson, 2002; Davidson et al., 2006; Diamond, 2002; Kolb et al., 2012; Luna, 2009). Thus, it would be beneficial to generalize our CPM analysis pipeline to developmental data, leveraging datasets like the ABCD Study® to investigate the neurodevelopmental trajectories of each facet of cognitive control. A thorough understanding of how the connectome of cognitive control components evolve across different ages could illuminate the origins of executive control and provide insights into the neural signatures of atypical cognitive control development.

**Funding Information**
Data were provided [in part] by the Human Connectome Project, WU-Minn Consortium (Principal Investigators: David Van Essen and Kamil Ugurbil; 1U54MH091657) funded by the 16 NIH Institutes and Centers that support the NIH Blueprint for Neuroscience Research; and by the McDonnell Center for Systems Neuroscience at Washington University. General attention connectome-based predictive model funded by National Institutes of Health, Grant Number MH108591 to M. M. C. Computing resources and S.Q. funded by Yale University.

**Author Contribution**
Shijie Qu: Conceptualization; Data Curation; Formal Analysis; Methodology; Project Administration; Software; Writing – Original Draft; Writing – Review & Editing. Yueyue Lydia Qu: Software; Writing – Review & Editing. Kwangsun Yoo: Methodology; Software; Supervision; Visualization; Writing – Review & Editing. Marvin M. Chun: Conceptualization; Funding Acquisition; Methodology; Project Administration; Supervision; Writing – Review & Editing.

Corresponding authors: Shijie Qu, Department of Psychology, Yale University, USA, or via e-mail: shijie.qu@yale.edu; Kwangsun Yoo, Department of Digital Health; Sungkyunkwan University, South Korea, or e-mail: rayksyoo@skku.edu; Marvin M. Chun, Department of Psychology, Yale University, USA, or via e-mail: marvin.chun@yale.edu.

## Tables

**Table 1.** Pearson Correlation between behavior measures

| | Flanker | Card Sort | 2-back |
|---|---|---|---|
| Flanker | -- | -- | -- |
| Card Sort | 0.4905$^{***}$ | -- | -- |
| 2-back | 0.3094$^{***}$ | 0.3525$^{***}$ | -- |

$^{***}p<0.001$, uncorrected

**Table 2.** CPM prediction accuracy of raw cognitive control measures, grayordinate

| | | *Working Memory (2-back)* | | | *Rest* | | |
|---|---|---|---|---|---|---|---|
| | | Flanker | Card Sort | 2-Back | Flanker | Card Sort | 2-Back |
| Positive | Flanker | 0.23$^{***}$ | 0.18$^{***}$ | 0.35$^{***}$ | 0.16$^{*,a}$ | 0.13$^{\dagger,b}$ | 0.32$^{***}$ |
| | Card Sort | 0.20$^{***}$ | 0.26$^{***}$ | 0.35$^{***}$ | 0.16$^{*,c}$ | 0.21$^{***}$ | 0.26$^{***}$ |
| | 2-Back | 0.24$^{***}$ | 0.23$^{***}$ | 0.42$^{***}$ | 0.21$^{***}$ | 0.18$^{***}$ | 0.37$^{***}$ |
| Negative | Flanker | 0.28$^{***}$ | 0.20$^{***}$ | 0.34$^{***}$ | 0.20$^{***}$ | 0.13$^{\dagger,d}$ | 0.27$^{***}$ |
| | Card Sort | 0.25$^{***}$ | 0.31$^{***}$ | 0.36$^{***}$ | 0.16$^{*,e}$ | 0.20$^{***}$ | 0.25$^{***}$ |
| | 2-Back | 0.28$^{***}$ | 0.27$^{***}$ | 0.44$^{***}$ | 0.23$^{***}$ | 0.18$^{***}$ | 0.35$^{***}$ |
| Both | Flanker | 0.29$^{***}$ | 0.21$^{***}$ | 0.36$^{***}$ | 0.20$^{***}$ | 0.14$^{*,f}$ | 0.31$^{***}$ |
| | Card Sort | 0.25$^{***}$ | 0.32$^{***}$ | 0.39$^{***}$ | 0.18$^{***}$ | 0.23$^{***}$ | 0.29$^{***}$ |
| | 2-Back | 0.29$^{***}$ | 0.28$^{***}$ | 0.48$^{***}$ | 0.25$^{***}$ | 0.20$^{***}$ | 0.39$^{***}$ |

Each sub-table (bounded by bold lines) represents a set of CPM prediction performance scores for a specific fMRI task state (2-back working memory vs. rest) using one type of edges (positive, negative, or both). For example, the top-left sub-table shows the CPM performance using working memory task fMRI data and only positive-associated edges. In each 3x3 sub-table, each row represents the training behavior, and each column represents the testing behavior. The maximums of each row and column in the sub-tables are colored in blue and yellow, respectively, with the overlap colored in green. $^{***}p<0.001$, $^{**}p<0.01$; $^{*}p<0.05$; $^{\dagger}p<0.1$, all corrected for family-wise error (FWE) after permutation testing. Exact p-values: $^{a}$: $p=0.012$; $^{b}$: $p=0.060$; $^{c}$: $p=0.024$; $^{d}$: $p=0.072$; $^{e}$: $p=0.012$; $^{f}$: $p=0.012$.

**Table 3.** CPM prediction accuracy of general and specific control measures, grayordinate

| | | General Control | Flanker Specific | Card Sort Specific | 2-Back Specific |
|---|---|---|---|---|---|
| Positive | General Control | 0.39$^{***}$ | 0.10$^{a}$ | 0.06$^{b}$ | 0.30$^{***}$ |
| | Flanker Specific | 0.17$^{*,c}$ | 0.13$^{\dagger,d}$ | -0.07$^{e}$ | 0.15$^{*,f}$ |
| | Card Sort Specific | 0.13$^{g}$ | -0.06$^{h}$ | 0.16$^{**,i}$ | 0.04$^{j}$ |
| | 2-Back Specific | 0.31$^{***}$ | 0.04$^{k}$ | -0.01$^{l}$ | 0.36$^{***}$ |
| Negative | General Control | 0.45$^{***}$ | 0.12$^{m}$ | 0.08$^{n}$ | 0.33$^{***}$ |
| | Flanker Specific | 0.15$^{*,o}$ | 0.12$^{p}$ | -0.05$^{q}$ | 0.11$^{r}$ |
| | Card Sort Specific | 0.10$^{s}$ | -0.07$^{t}$ | 0.16$^{*,u}$ | 0.02$^{v}$ |
| | 2-Back Specific | 0.38$^{***}$ | 0.08$^{w}$ | 0.04$^{x}$ | 0.34$^{***}$ |
| Both | General Control | 0.46$^{***}$ | 0.12$^{y}$ | 0.08$^{z}$ | 0.34$^{***}$ |
| | Flanker Specific | 0.18$^{***}$ | 0.15$^{*,aa}$ | -0.07$^{ab}$ | 0.15$^{\dagger,ac}$ |
| | Card Sort Specific | 0.13$^{ad}$ | -0.08$^{ae}$ | 0.18$^{**,af}$ | 0.03$^{ag}$ |
| | 2-Back Specific | 0.40$^{***}$ | 0.07$^{ah}$ | 0.02$^{ai}$ | 0.40$^{***}$ |

Each sub-table (bounded by horizontal lines) corresponds to the CPM prediction performance scores using 2-back task-fMRI and one type of edges (positive, negative, or both). In every 4x4 sub-table, each row represents the training behavior, and each column represents the testing behavior. The maximums of each row and column in the sub-tables are colored in blue and yellow, respectively, with the overlap colored in green. $^{***}p<0.001$, $^{**}p<0.01$; $^{*}p<0.05$; $^{\dagger}p<0.1$, all corrected for family-wise error (FWE) after permutation testing. Exact p-values: $^{a}$: $p$=0.79; $^{b}$: $p$=3.50; $^{c}$: $p$=0.024; $^{d}$: $p$=0.064; $^{e}$: $p$=2.59; $^{f}$: $p$=0.024; $^{g}$: $p$=0.12; $^{h}$: $p$=3.41; $^{i}$: $p$=0.008; $^{j}$: $p$=6.14; $^{k}$: $p$=5.71; $^{l}$: $p$=10.92; $^{m}$: $p$=0.33; $^{n}$: $p$=2.23; $^{o}$: $p$=0.024; $^{p}$: $p$=0.13; $^{q}$: $p$=4.56; $^{r}$: $p$=0.53; $^{s}$: $p$=1.18; $^{t}$: $p$=2.76; $^{u}$: $p$=0.024; $^{v}$: $p$=10.03; $^{w}$: $p$=2.40; $^{x}$: $p$=6.17; $^{y}$: $p$=0.38; $^{z}$: $p$=1.90; $^{aa}$: $p$=0.048; $^{ab}$: $p$=2.33; $^{ac}$: $p$=0.072; $^{ad}$: $p$=0.24; $^{ae}$: $p$=1.90; $^{af}$: $p$=0.008; $^{ag}$: $p$=8.09; $^{ah}$: $p$=2.57; $^{ai}$: $p$=8.93.

## Figures

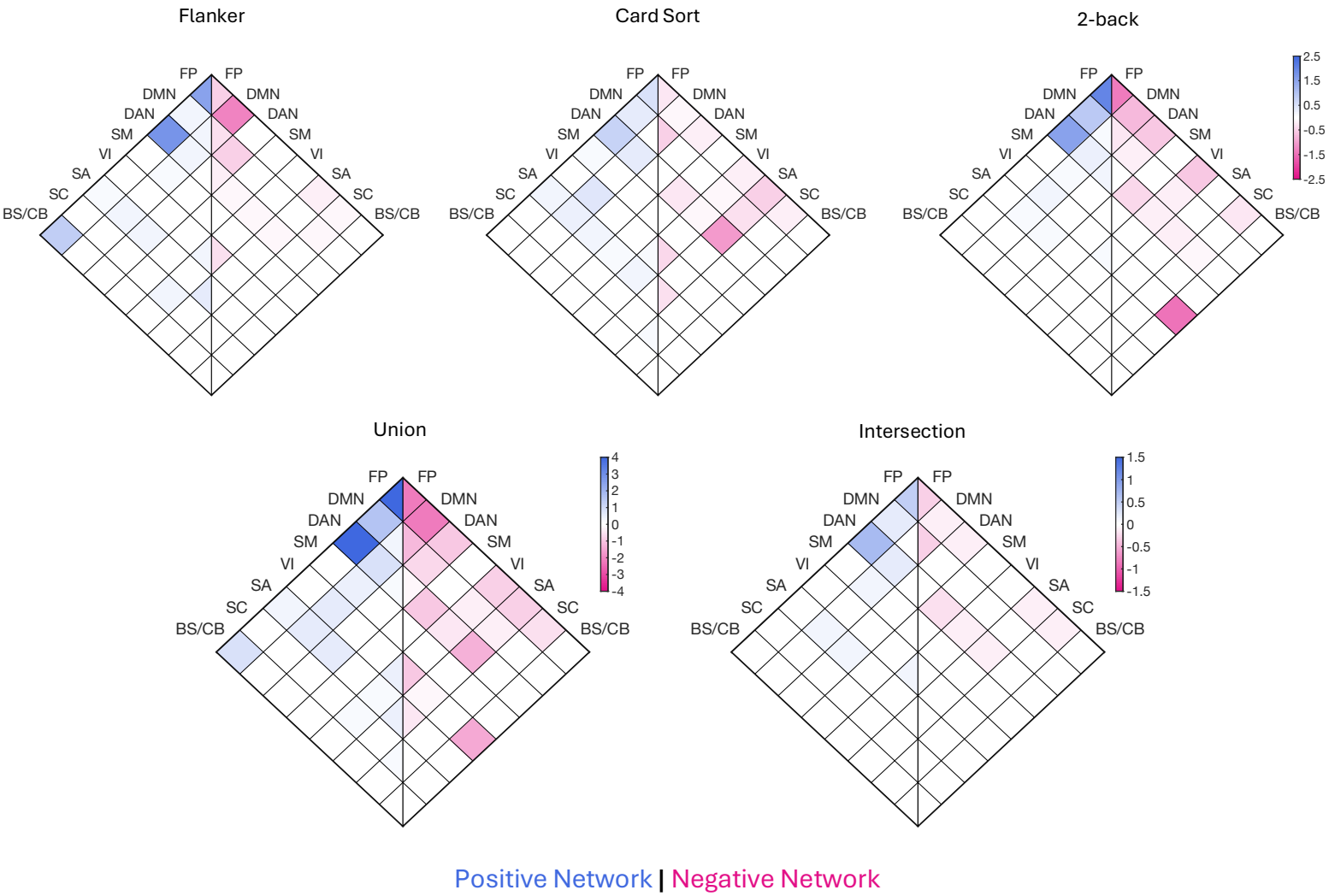


**Figure 1. Predictive edges identified by CPM on three control measures.** The top row displays the edges identified by CPMs trained on each of the three types of cognitive control measures. Each heatmap is divided into left and right halves, where the right half represents negative edges, and the left half represents positive edges. Each cell within the heatmap indicates the percentage of reliable edges (see the Methods section for detailed inclusion criteria) identified between the corresponding pair of canonical networks. Higher percentages are represented by more intense pink or blue hues. The bottom row illustrates the union (sum) and intersection (minimum) of the three heatmaps above. FP, frontoparietal; DM, default mode; DA, dorsal attention; SM, somatomotor; VI, visual; SA, salience; SC, subcortical; BS/CB, brain stem/cerebellum.

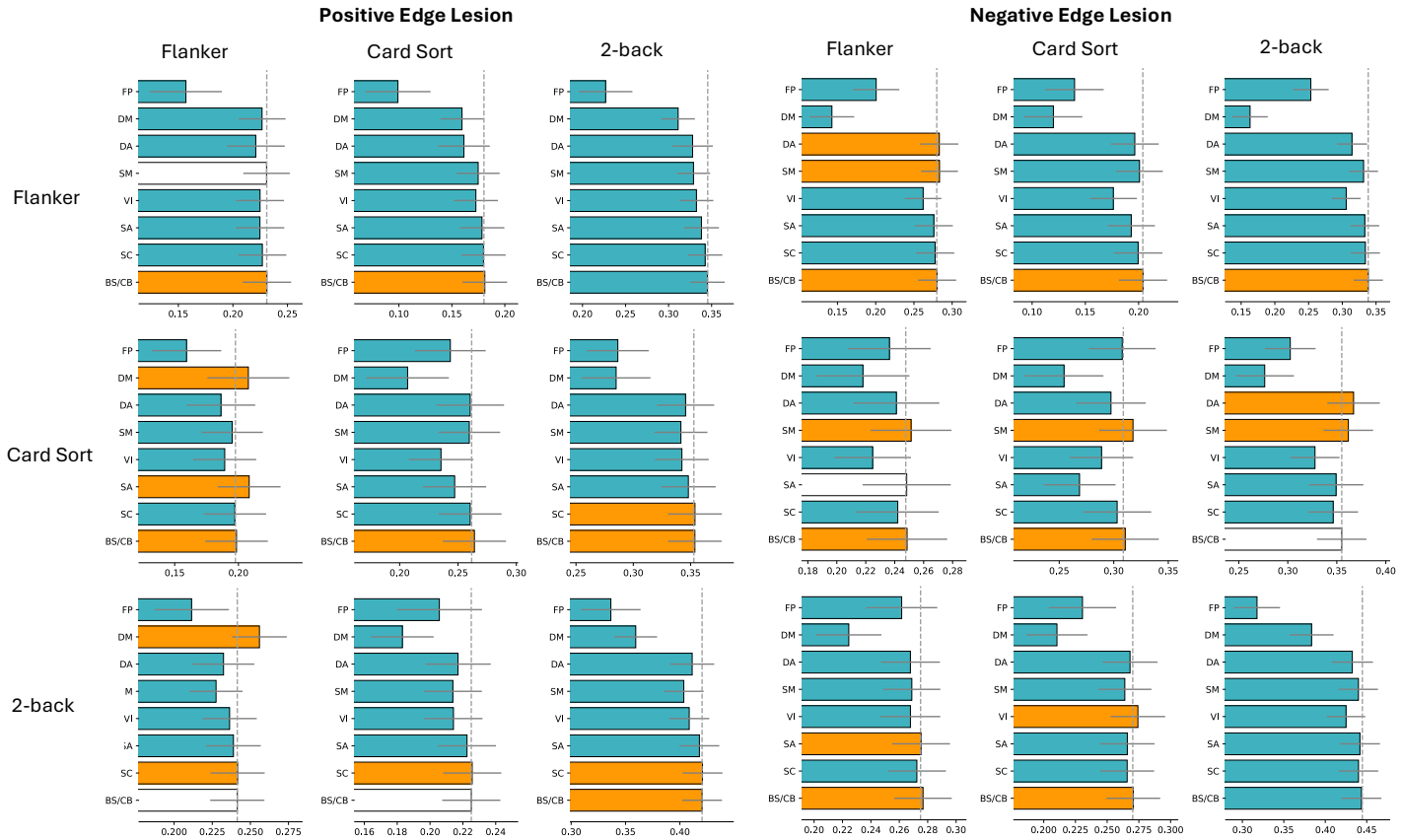


**Figure 2. CPM lesion analysis on grayordinate, 2-back task-fMRI data.** The figure is divided into two main sections: the left half displays CPM performance after lesioning positive edges of each network, while the right half shows the results after lesioning negative edges. Each section is further divided into subplots based on different train/test task combinations. In these subplots, each row corresponds to a training task, and each column represents a testing task. For example, the top-left subplot in the left half illustrates CPM prediction when trained and tested both on the Flanker scores after lesioning positive edges of each canonical network. The horizontal gray line attached to each bar denotes the 95% ($\pm$ 2 standard deviation) confidence interval. The vertical gray dashed line represents the baseline CPM performance (without lesioning) for each scenario. To assess the impact of lesioning, paired t-tests were conducted comparing the lesioned performance to the regular performance. The results are depicted with colored bars: blue bars indicate significant reductions in performance ($p$<0.05, after FWE correction), orange bars represent significant increases, and white bars denote no significant difference from regular performance. All significant bars except the within-Card Sort prediction in the frontoparietal negative edge lesion condition have $p$<0.001 (FWE corrected). The within-Card Sort prediction when lesioning FP negative edges has $p$ = 0.037. For non-significant conditions (white bars): Flanker-Flanker, SM, positive ($p$=5.96); 2Back-Flanker, BS/CB, positive ($p$=43.17); 2Back-Card Sort, BS/CB, positive ($p$=0.078); Card Sort-Flanker, SA, negative ($p$=0.37); Card Sort-2Back, BS/CB, negative ($p$=15.30). FP, frontoparietal; DM, default mode; DA, dorsal attention; SM, somatomotor; VI, visual; SA, salience; SC, subcortical; BS/CB, brain stem/cerebellum.

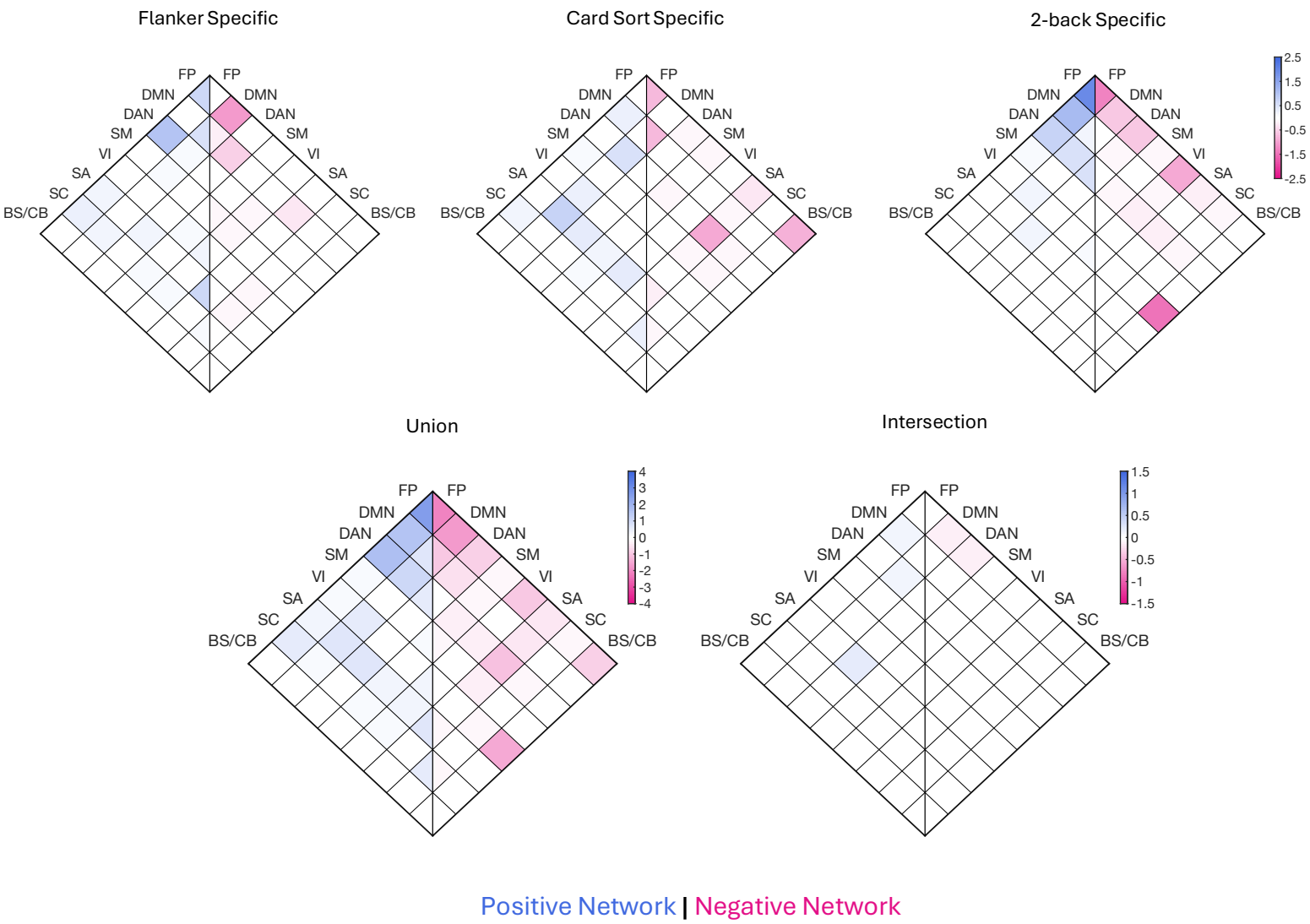


**Figure 3. Predictive edges identified by CPM on the three component-specific measures.** The top row displays the edges identified by CPMs trained on each of the three component-specific measures. The bottom row illustrates the union (sum) and intersection (minimum) of the three heatmaps above. FP, frontoparietal; DM, default mode; DA, dorsal attention; SM, somatomotor; VI, visual; SA, salience; SC, subcortical; BS/CB, brain stem/cerebellum.

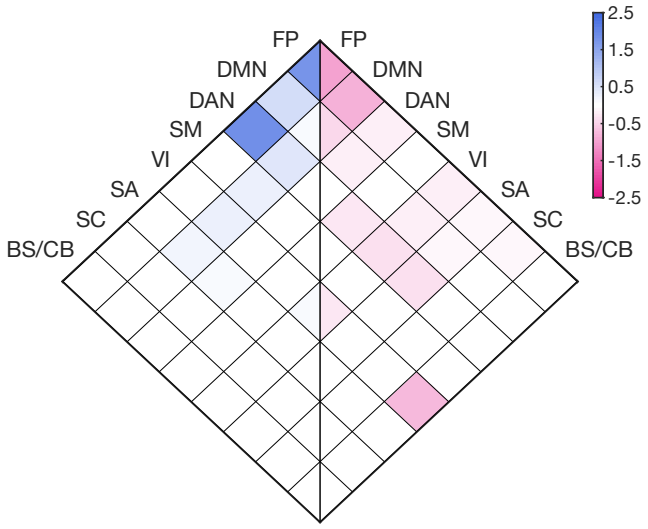


Positive Network | Negative Network

**Figure 4. Predictive edges identified by CPM on the general cognitive control measure**. FP, frontoparietal; DM, default mode; DA, dorsal attention; SM, somatomotor; VI, visual; SA, salience; SC, subcortical; BS/CB, brain stem/cerebellum.

## Reference


Anderson, P. (2002). Assessment and Development of Executive Function (EF) During Childhood. *Child Neuropsychology*, *8*(2), 71–82. https://doi.org/10.1076/chin.8.2.71.8724

Aron, A. R., Fletcher, P. C., Bullmore, E. T., Sahakian, B. J., & Robbins, T. W. (2003). Stop-signal inhibition disrupted by damage to right inferior frontal gyrus in humans. *Nature Neuroscience*, *6*(2), 115–116. https://doi.org/10.1038/nn1003

Aron, A. R., Monsell, S., Sahakian, B. J., & Robbins, T. W. (2004). A componential analysis of task-switching deficits associated with lesions of left and right frontal cortex. *Brain*, *127*(7), 1561–1573. https://doi.org/10.1093/brain/awh169

Assem, M., Shashidhara, S., Glasser, M. F., & Duncan, J. (2024). Basis of executive functions in fine-grained architecture of cortical and subcortical human brain networks. *Cerebral Cortex*, bhad537. https://doi.org/10.1093/cercor/bhad537

Avery, E. W., Yoo, K., Rosenberg, M. D., Greene, A. S., Gao, S., Na, D. L., Scheinost, D., Constable, T. R., & Chun, M. M. (2020). Distributed Patterns of Functional Connectivity Predict Working Memory Performance in Novel Healthy and Memory-impaired Individuals. *Journal of Cognitive Neuroscience*, *32*(2), 241–255. https://doi.org/10.1162/jocn_a_01487

Baddeley, A., Chincotta, D., & Adlam, A. (2001). Working memory and the control of action: Evidence from task switching. *Journal of Experimental Psychology: General*, *130*(4), 641–657. https://doi.org/10.1037/0096-3445.130.4.641

Baldassarre, A., Lewis, C. M., Committeri, G., Snyder, A. Z., Romani, G. L., & Corbetta, M. (2012). Individual variability in functional connectivity predicts performance of a perceptual task. *Proceedings of the National Academy of Sciences*, *109*(9), 3516–3521. https://doi.org/10.1073/pnas.1113148109

Barbey, A. K., Koenigs, M., & Grafman, J. (2013). Dorsolateral prefrontal contributions to human working memory. *Cortex*, *49*(5), 1195–1205. https://doi.org/10.1016/j.cortex.2012.05.022

Beaty, R. E., Kenett, Y. N., Christensen, A. P., Rosenberg, M. D., Benedek, M., Chen, Q., Fink, A., Qiu, J., Kwapil, T. R., Kane, M. J., & Silvia, P. J. (2018). Robust prediction of individual creative ability from brain functional connectivity. *Proceedings of the National Academy of Sciences*, *115*(5), 1087–1092. https://doi.org/10.1073/pnas.1713532115

Berg, E. A. (1948). A simple objective technique for measuring flexibility in thinking. *The Journal of General Psychology*, *39*, 15–22. https://doi.org/10.1080/00221309.1948.9918159

Brodoehl, S., Gaser, C., Dahnke, R., Witte, O. W., & Klingner, C. M. (2020). Surface-based analysis increases the specificity of cortical activation patterns and connectivity results. *Scientific Reports*, *10*(1), 5737. https://doi.org/10.1038/s41598-020-62832-z

Burgess, P. W. (1997). Theory and Methodology in Executive Function Research. In *Methodology Of Frontal And Executive Function*. Routledge.

Carter, C. S., & van Veen, V. (2007). Anterior cingulate cortex and conflict detection: An update of theory and data. *Cognitive, Affective, & Behavioral Neuroscience*, *7*(4), 367–379. https://doi.org/10.3758/CABN.7.4.367

Chén, O. Y., Cao, H., Reinen, J. M., Qian, T., Gou, J., Phan, H., De Vos, M., & Cannon, T. D. (2019). Resting-state brain information flow predicts cognitive flexibility in humans. *Scientific Reports*, *9*(1), 3879. https://doi.org/10.1038/s41598-019-40345-8

Cole, M. W., Yarkoni, T., Repovs, G., Anticevic, A., & Braver, T. S. (2012). Global Connectivity of Prefrontal Cortex Predicts Cognitive Control and Intelligence. *Journal of Neuroscience*, *32*(26), 8988–8999. https://doi.org/10.1523/JNEUROSCI.0536-12.2012

Conway, A. R., Cowan, N., & Bunting, M. F. (2001). The cocktail party phenomenon revisited: The importance of working memory capacity. *Psychonomic Bulletin & Review*, *8*(2), 331–335. https://doi.org/10.3758/bf03196169

Corbetta, M., & Shulman, G. L. (2002). Control of goal-directed and stimulus-driven attention in the brain. *Nature Reviews Neuroscience*, *3*(3), 201–215. https://doi.org/10.1038/nrn755

Corbetta, M., & Shulman, G. L. (2011). Spatial Neglect and Attention Networks. *Annual Review of Neuroscience*, *34*(Volume 34, 2011), 569–599. https://doi.org/10.1146/annurev-neuro-061010-113731

Dajani, D. R., & Uddin, L. Q. (2015). Demystifying cognitive flexibility: Implications for clinical and developmental neuroscience. *Trends in Neurosciences*, *38*(9), 571–578. https://doi.org/10.1016/j.tins.2015.07.003

Davidson, M. C., Amso, D., Anderson, L. C., & Diamond, A. (2006). Development of cognitive control and executive functions from 4 to 13 years: Evidence from manipulations of memory, inhibition, and task switching. *Neuropsychologia*, *44*(11), 2037–2078. https://doi.org/10.1016/j.neuropsychologia.2006.02.006

Deck, B. L., Kelkar, A., Erickson, B., Erani, F., McConathey, E., Sacchetti, D., Faseyitan, O., Hamilton, R., & Medaglia, J. D. (2023). Individual-level functional connectivity predicts cognitive control efficiency. *NeuroImage*, *283*, 120386. https://doi.org/10.1016/j.neuroimage.2023.120386

Derrfuss, J., Brass, M., Neumann, J., & von Cramon, D. Y. (2005). Involvement of the inferior frontal junction in cognitive control: Meta-analyses of switching and Stroop studies. *Human Brain Mapping*, *25*(1), 22–34. https://doi.org/10.1002/hbm.20127

Diamond, A. (2002). Normal Development of Prefrontal Cortex from Birth to Young Adulthood: Cognitive Functions, Anatomy, and Biochemistry. In D. T. Stuss & R. T. Knight (Eds.), *Principles of Frontal Lobe Function* (p. 0). Oxford University Press. https://doi.org/10.1093/acprof:oso/9780195134971.003.0029

Diamond, A. (2013). Executive Functions. *Annual Review of Psychology*, *64*, 135–168. https://doi.org/10.1146/annurev-psych-113011-143750

Dixon, M. L., De La Vega, A., Mills, C., Andrews-Hanna, J., Spreng, R. N., Cole, M. W., & Christoff, K. (2018). Heterogeneity within the frontoparietal control network and its relationship to the default and dorsal attention networks. *Proceedings of the National Academy of Sciences*, *115*(7), E1598–E1607. https://doi.org/10.1073/pnas.1715766115

Dosenbach, N. U. F., Fair, D. A., Cohen, A. L., Schlaggar, B. L., & Petersen, S. E. (2008). A dual-networks architecture of top-down control. *Trends in Cognitive Sciences*, *12*(3), 99–105. https://doi.org/10.1016/j.tics.2008.01.001

Elliott, M. L., Knodt, A. R., Cooke, M., Kim, M. J., Melzer, T. R., Keenan, R., Ireland, D., Ramrakha, S., Poulton, R., Caspi, A., Moffitt, T. E., & Hariri, A. R. (2019). General functional connectivity: Shared features of resting-state and task fMRI drive reliable and heritable individual differences in functional brain networks. *NeuroImage*, *189*, 516–532. https://doi.org/10.1016/j.neuroimage.2019.01.068

Elton, A., & Gao, W. (2015). Task-positive Functional Connectivity of the Default Mode Network Transcends Task Domain. *Journal of Cognitive Neuroscience*, *27*(12), 2369–2381. https://doi.org/10.1162/jocn_a_00859

Emerson, M. J., & Miyake, A. (2003). The role of inner speech in task switching: A dual-task investigation. *Journal of Memory and Language*, *48*(1), 148–168. https://doi.org/10.1016/S0749-596X(02)00511-9

Engle, R. W. (2002). Working Memory Capacity as Executive Attention. *Current Directions in Psychological Science*, *11*(1), 19–23. https://doi.org/10.1111/1467-8721.00160

Engle, R. W., Tuholski, S. W., Laughlin, J. E., & Conway, A. R. A. (1999). Working memory, short-term memory, and general fluid intelligence: A latent-variable approach. *Journal of Experimental Psychology: General*, *128*(3), 309–331. https://doi.org/10.1037/0096-3445.128.3.309

Eriksen, B. A., & Eriksen, C. W. (1974). Effects of noise letters upon the identification of a target letter in a nonsearch task. *Perception & Psychophysics*, *16*(1), 143–149. https://doi.org/10.3758/BF03203267

Finn, E. S., & Bandettini, P. A. (2021). Movie-watching outperforms rest for functional connectivity-based prediction of behavior. *NeuroImage*, *235*, 117963. https://doi.org/10.1016/j.neuroimage.2021.117963

Finn, E. S., Shen, X., Scheinost, D., Rosenberg, M. D., Huang, J., Chun, M. M., Papademetris, X., & Constable, R. T. (2015). Functional connectome fingerprinting: Identifying individuals using patterns of brain connectivity. *Nature Neuroscience*, *18*(11), 1664–1671. https://doi.org/10.1038/nn.4135

Floden, D., & Stuss, D. T. (2006). Inhibitory Control is Slowed in Patients with Right Superior Medial Frontal Damage. *Journal of Cognitive Neuroscience*, *18*(11), 1843–1849. https://doi.org/10.1162/jocn.2006.18.11.1843

Friedman, N. P., & Miyake, A. (2017). Unity and diversity of executive functions: Individual differences as a window on cognitive structure. *Cortex*, *86*, 186–204. https://doi.org/10.1016/j.cortex.2016.04.023

Friedman, N. P., Miyake, A., Corley, R. P., Young, S. E., DeFries, J. C., & Hewitt, J. K. (2006). Not All Executive Functions Are Related to Intelligence. *Psychological Science*, *17*(2), 172–179. https://doi.org/10.1111/j.1467-9280.2006.01681.x

Friedman, N. P., & Robbins, T. W. (2022a). The role of prefrontal cortex in cognitive control and executive function. *Neuropsychopharmacology*, *47*(1), 72–89. https://doi.org/10.1038/s41386-021-01132-0

Friedman, N. P., & Robbins, T. W. (2022b). The role of prefrontal cortex in cognitive control and executive function. *Neuropsychopharmacology*, *47*(1), 72–89. https://doi.org/10.1038/s41386-021-01132-0

Frye, D., Zelazo, P. D., & Palfai, T. (1995). Theory of mind and rule-based reasoning. *Cognitive Development*, *10*(4), 483–527. https://doi.org/10.1016/0885-2014(95)90024-1

Glasser, M. F., Sotiropoulos, S. N., Wilson, J. A., Coalson, T. S., Fischl, B., Andersson, J. L., Xu, J., Jbabdi, S., Webster, M., Polimeni, J. R., Van Essen, D. C., & Jenkinson, M. (2013). The minimal preprocessing pipelines for the Human Connectome Project. *NeuroImage*, *80*, 105–124. https://doi.org/10.1016/j.neuroimage.2013.04.127

Greene, A. S., Gao, S., Noble, S., Scheinost, D., & Constable, R. T. (2020). How Tasks Change Whole-Brain Functional Organization to Reveal Brain-Phenotype Relationships. *Cell Reports*, *32*(8), 108066. https://doi.org/10.1016/j.celrep.2020.108066

Greene, A. S., Gao, S., Scheinost, D., & Constable, R. T. (2018). Task-induced brain state manipulation improves prediction of individual traits. *Nature Communications*, *9*(1), 2807. https://doi.org/10.1038/s41467-018-04920-3

Hayes, A. E., Davidson, M. C., Keele, S. W., & Rafal, R. D. (1998). Toward a functional analysis of the basal ganglia. *Journal of Cognitive Neuroscience*, *10*(2), 178–198. https://doi.org/10.1162/089892998562645

He, B. J., Snyder, A. Z., Vincent, J. L., Epstein, A., Shulman, G. L., & Corbetta, M. (2007). Breakdown of functional connectivity in frontoparietal networks underlies behavioral deficits in spatial neglect. *Neuron*, *53*(6), 905–918. https://doi.org/10.1016/j.neuron.2007.02.013

Huijbers, W., Van Dijk, K. R. A., Boenniger, M. M., Stirnberg, R., & Breteler, M. M. B. (2017). Less head motion during MRI under task than resting-state conditions. *NeuroImage*, *147*, 111–120. https://doi.org/10.1016/j.neuroimage.2016.12.002

Isaacs, E. B., & Vargha-Khadem, F. (1989). Differential course of development of spatial and verbal memory span: A normative study. *British Journal of Developmental Psychology*, *7*(4), 377–380. https://doi.org/10.1111/j.2044-835X.1989.tb00814.x

Jiang, R., Zuo, N., Ford, J. M., Qi, S., Zhi, D., Zhuo, C., Xu, Y., Fu, Z., Bustillo, J., Turner, J. A., Calhoun, V. D., & Sui, J. (2020). Task-induced brain connectivity promotes the detection of individual differences in brain-behavior relationships. *NeuroImage*, *207*, 116370. https://doi.org/10.1016/j.neuroimage.2019.116370

Kane, M. J., Brown, L. H., McVay, J. C., Silvia, P. J., Myin-Germeys, I., & Kwapil, T. R. (2007). For whom the mind wanders, and when: An experience-sampling study of working memory and executive control in daily life. *Psychological Science*, *18*(7), 614–621. https://doi.org/10.1111/j.1467-9280.2007.01948.x

Kane, M. J., & Engle, R. W. (2003). Working-memory capacity and the control of attention: The contributions of goal neglect, response competition, and task set to Stroop interference. *Journal of Experimental Psychology: General*, *132*(1), 47–70. https://doi.org/10.1037/0096-3445.132.1.47

Kim, C., Cilles, S. E., Johnson, N. F., & Gold, B. T. (2012). Domain general and domain preferential brain regions associated with different types of task switching: A meta-

analysis. *Human Brain Mapping*, *33*(1), 130–142. https://doi.org/10.1002/hbm.21199

Kirchner, W. K. (1958). Age differences in short-term retention of rapidly changing information. *Journal of Experimental Psychology*, *55*(4), 352–358. https://doi.org/10.1037/h0043688

Koch, I., Gade, M., Schuch, S., & Philipp, A. M. (2010). The role of inhibition in task switching: A review. *Psychonomic Bulletin & Review*, *17*(1), 1–14. https://doi.org/10.3758/PBR.17.1.1

Kolb, B., Mychasiuk, R., Muhammad, A., Li, Y., Frost, D. O., & Gibb, R. (2012). Experience and the developing prefrontal cortex. *Proceedings of the National Academy of Sciences of the United States of America*, *109*(Suppl 2), 17186–17193. https://doi.org/10.1073/pnas.1121251109

Kristo, G., Rutten, G.-J., Raemaekers, M., de Gelder, B., Rombouts, S. A. R. B., & Ramsey, N. F. (2014). Task and task-free FMRI reproducibility comparison for motor network identification. *Human Brain Mapping*, *35*(1), 340–352. https://doi.org/10.1002/hbm.22180

Leech, R., Kamourieh, S., Beckmann, C. F., & Sharp, D. J. (2011). Fractionating the default mode network: Distinct contributions of the ventral and dorsal posterior cingulate cortex to cognitive control. *The Journal of Neuroscience: The Official Journal of the Society for Neuroscience*, *31*(9), 3217–3224. https://doi.org/10.1523/JNEUROSCI.5626-10.2011

Lehto, J. E., Juujärvi, P., Kooistra, L., & Pulkkinen, L. (2003). Dimensions of executive functioning: Evidence from children. *British Journal of Developmental Psychology*, *21*(1), 59–80. https://doi.org/10.1348/026151003321164627

Lemire-Rodger, S., Lam, J., Viviano, J. D., Stevens, W. D., Spreng, R. N., & Turner, G. R. (2019). Inhibit, switch, and update: A within-subject fMRI investigation of executive control. *Neuropsychologia*, *132*, 107134. https://doi.org/10.1016/j.neuropsychologia.2019.107134

Logan, G. D., & Cowan, W. B. (1984). On the ability to inhibit thought and action: A theory of an act of control. *Psychological Review*, *91*(3), 295–327. https://doi.org/10.1037/0033-295X.91.3.295

Luna, B. (2009). Developmental Changes in Cognitive Control through Adolescence. In P. Bauer (Ed.), *Advances in Child Development and Behavior* (Vol. 37, pp. 233–278). JAI. https://doi.org/10.1016/S0065-2407(09)03706-9

Marek, S., & Dosenbach, N. U. F. (2018). The frontoparietal network: Function, electrophysiology, and importance of individual precision mapping. *Dialogues in Clinical Neuroscience*, *20*(2), 133–140. https://doi.org/10.31887/DCNS.2018.20.2/smarek

Mayr, U., & Keele, S. W. (2000). Changing internal constraints on action: The role of backward inhibition. *Journal of Experimental Psychology. General*, *129*(1), 4–26. https://doi.org/10.1037//0096-3445.129.1.4

McNab, F., Leroux, G., Strand, F., Thorell, L., Bergman, S., & Klingberg, T. (2008). Common and unique components of inhibition and working memory: An fMRI, within-subjects

investigation. *Neuropsychologia*, *46*(11), 2668–2682. https://doi.org/10.1016/j.neuropsychologia.2008.04.023

Menon, V., & D'Esposito, M. (2022). The role of PFC networks in cognitive control and executive function. *Neuropsychopharmacology*, *47*(1), 90–103. https://doi.org/10.1038/s41386-021-01152-w

Menon, V., & Uddin, L. Q. (2010). Saliency, switching, attention and control: A network model of insula function. *Brain Structure & Function*, *214*(5–6), 655–667. https://doi.org/10.1007/s00429-010-0262-0

Miller, K. M., Price, C. C., Okun, M. S., Montijo, H., & Bowers, D. (2009). Is the N-Back Task a Valid Neuropsychological Measure for Assessing Working Memory? *Archives of Clinical Neuropsychology*, *24*(7), 711–717. https://doi.org/10.1093/arclin/acp063

Miyake, A., & Friedman, N. P. (2012). The Nature and Organization of Individual Differences in Executive Functions: Four General Conclusions. *Current Directions in Psychological Science*, *21*(1), 8–14. https://doi.org/10.1177/0963721411429458

Miyake, A., Friedman, N. P., Emerson, M. J., Witzki, A. H., Howerter, A., & Wager, T. D. (2000). The Unity and Diversity of Executive Functions and Their Contributions to Complex "Frontal Lobe" Tasks: A Latent Variable Analysis. *Cognitive Psychology*, *41*(1), 49–100. https://doi.org/10.1006/cogp.1999.0734

Mj, K., & Rw, E. (2003). Working-memory capacity and the control of attention: The contributions of goal neglect, response competition, and task set to Stroop interference. *Journal of Experimental Psychology. General*, *132*(1). https://doi.org/10.1037/0096-3445.132.1.47

Niendam, T. A., Laird, A. R., Ray, K. L., Dean, Y. M., Glahn, D. C., & Carter, C. S. (2012). Meta-analytic evidence for a superordinate cognitive control network subserving diverse executive functions. *Cognitive, Affective, & Behavioral Neuroscience*, *12*(2), 241–268. https://doi.org/10.3758/s13415-011-0083-5

Phillips, L. H. (1997). Do "Frontal Tests" Measure Executive Function? Issues of Assessment and Evidence from Fluency Tests. In *Methodology Of Frontal And Executive Function*. Routledge.

Reineberg, A. E., Andrews-Hanna, J. R., Depue, B. E., Friedman, N. P., & Banich, M. T. (2015). Resting-state networks predict individual differences in common and specific aspects of executive function. *NeuroImage*, *104*, 69–78. https://doi.org/10.1016/j.neuroimage.2014.09.045

Reineberg, A. E., & Banich, M. T. (2016). Functional connectivity at rest is sensitive to individual differences in executive function: A network analysis. *Human Brain Mapping*, *37*(8), 2959–2975. https://doi.org/10.1002/hbm.23219

Rodríguez-Nieto, G., Seer, C., Sidlauskaite, J., Vleugels, L., Van Roy, A., Hardwick, R., & Swinnen, S. (2022). Inhibition, Shifting and Updating: Inter and intra-domain commonalities and differences from an executive functions activation likelihood estimation meta-analysis. *NeuroImage*, *264*, 119665. https://doi.org/10.1016/j.neuroimage.2022.119665

Rosazza, C., Aquino, D., D'Incerti, L., Cordella, R., Andronache, A., Zacà, D., Bruzzone, M. G., Tringali, G., & Minati, L. (2014). Preoperative Mapping of the Sensorimotor

Cortex: Comparative Assessment of Task-Based and Resting-State fMRI. *PLOS ONE*, *9*(6), e98860. https://doi.org/10.1371/journal.pone.0098860

Rosenberg, M. D., Finn, E. S., Scheinost, D., Papademetris, X., Shen, X., Constable, R. T., & Chun, M. M. (2016). A neuromarker of sustained attention from whole-brain functional connectivity. *Nature NEUROSCIENCE*, *19*(1).

Salimi-Khorshidi, G., Douaud, G., Beckmann, C. F., Glasser, M. F., Griffanti, L., & Smith, S. M. (2014). Automatic denoising of functional MRI data: Combining independent component analysis and hierarchical fusion of classifiers. *NeuroImage*, *90*, 449–468. https://doi.org/10.1016/j.neuroimage.2013.11.046

Schaefer, A., Kong, R., Gordon, E. M., Laumann, T. O., Zuo, X.-N., Holmes, A. J., Eickhoff, S. B., & Yeo, B. T. T. (2018). Local-Global Parcellation of the Human Cerebral Cortex from Intrinsic Functional Connectivity MRI. *Cerebral Cortex (New York, N.Y.: 1991)*, *28*(9), 3095–3114. https://doi.org/10.1093/cercor/bhx179

Seeley, W. W., Menon, V., Schatzberg, A. F., Keller, J., Glover, G. H., Kenna, H., Reiss, A. L., & Greicius, M. D. (2007). Dissociable intrinsic connectivity networks for salience processing and executive control. *The Journal of Neuroscience: The Official Journal of the Society for Neuroscience*, *27*(9), 2349–2356. https://doi.org/10.1523/JNEUROSCI.5587-06.2007

Shen, X., Finn, E. S., Scheinost, D., Rosenberg, M. D., Chun, M. M., Papademetris, X., & Constable, R. T. (2017). Using connectome-based predictive modeling to predict individual behavior from brain connectivity. *Nature Protocols*, *12*(3), 506–518. https://doi.org/10.1038/nprot.2016.178

Shen, X., Tokoglu, F., Papademetris, X., & Constable, R. T. (2013). Groupwise whole-brain parcellation from resting-state fMRI data for network node identification. *NeuroImage*, *82*, 403–415. https://doi.org/10.1016/j.neuroimage.2013.05.081

Smith, S. M., Andersson, J., Auerbach, E. J., Beckmann, C. F., Bijsterbosch, J., Douaud, G., Duff, E., Feinberg, D. A., Griffanti, L., Harms, M. P., Kelly, M., Laumann, T., Miller, K. L., Moeller, S., Petersen, S., Power, J., Salimi-Khorshidi, G., Snyder, A. Z., Vu, A., … Glasser, M. F. (2013). Resting-state fMRI in the Human Connectome Project. *NeuroImage*, *80*, 144–168. https://doi.org/10.1016/j.neuroimage.2013.05.039

Smolker, H. R., Depue, B. E., Reineberg, A. E., Orr, J. M., & Banich, M. T. (2015). Individual differences in regional prefrontal gray matter morphometry and fractional anisotropy are associated with different constructs of executive function. *Brain Structure & Function*, *220*(3), 1291–1306. https://doi.org/10.1007/s00429-014-0723-y

Sternberg, S. (1966). High-speed scanning in human memory. *Science (New York, N.Y.)*, *153*(3736), 652–654. https://doi.org/10.1126/science.153.3736.652

Stroop, J. R. (1935). Studies of interference in serial verbal reactions. *Journal of Experimental Psychology*, *18*(6), 643–662. https://doi.org/10.1037/h0054651

Tuominen, J., Specht, K., Vaisvilaite, L., & Zeidman, P. (2023). An information-theoretic analysis of resting-state versus task fMRI. *Network Neuroscience*, *7*(2), 769–786. https://doi.org/10.1162/netn_a_00302

Unsworth, N., Schrock, J. C., & Engle, R. W. (2004). Working Memory Capacity and the Antisaccade Task: Individual Differences in Voluntary Saccade Control. *Journal of*

*Experimental Psychology: Learning, Memory, and Cognition*, *30*(6), 1302–1321. https://doi.org/10.1037/0278-7393.30.6.1302

Van Essen, D. C., Ugurbil, K., Auerbach, E., Barch, D., Behrens, T. E. J., Bucholz, R., Chang, A., Chen, L., Corbetta, M., Curtiss, S. W., Della Penna, S., Feinberg, D., Glasser, M. F., Harel, N., Heath, A. C., Larson-Prior, L., Marcus, D., Michalareas, G., Moeller, S., … WU-Minn HCP Consortium. (2012). The Human Connectome Project: A data acquisition perspective. *NeuroImage*, *62*(4), 2222–2231. https://doi.org/10.1016/j.neuroimage.2012.02.018

Wang, J., Ren, Y., Hu, X., Nguyen, V. T., Guo, L., Han, J., & Guo, C. C. (2017). Test–retest reliability of functional connectivity networks during naturalistic fMRI paradigms. *Human Brain Mapping*, *38*(4), 2226–2241. https://doi.org/10.1002/hbm.23517

Yoo, K., Rosenberg, M. D., Hsu, W.-T., Zhang, S., Li, C.-S. R., Scheinost, D., Constable, R. T., & Chun, M. M. (2018). Connectome-based predictive modeling of attention: Comparing different functional connectivity features and prediction methods across datasets. *NeuroImage*, *167*, 11–22. https://doi.org/10.1016/j.neuroimage.2017.11.010

Yoo, K., Rosenberg, M. D., Kwon, Y. H., Lin, Q., Avery, E. W., Sheinost, D., Constable, R. T., & Chun, M. M. (2022). A brain-based general measure of attention. *Nature Human Behaviour*, *6*(6), 782–795. https://doi.org/10.1038/s41562-022-01301-1

Yoo, K., Rosenberg, M. D., Kwon, Y. H., Scheinost, D., Constable, R. T., & Chun, M. M. (2022). A cognitive state transformation model for task-general and task-specific subsystems of the brain connectome. *NeuroImage*, *257*, 119279. https://doi.org/10.1016/j.neuroimage.2022.119279

Yoo, K., Rosenberg, M. D., Noble, S., Scheinost, D., Constable, R. T., & Chun, M. M. (2019). Multivariate approaches improve the reliability and validity of functional connectivity and prediction of individual behaviors. *NeuroImage*, *197*, 212–223. https://doi.org/10.1016/j.neuroimage.2019.04.060

NIH Toolbox Scoring and interpretation guide - epicrehab. (n.d.). https://www.epicrehab.com/epic/documents/crc/crc-201307-nih-toolbox-scoring-and-interpretation-manual%209-27-12.pdf

## Supplementary Materials

**Supplementary Table 1.** Statistics of raw behavior measures

| | Flanker | Card Sort | 2-Back |
|---|---|---|---|
| count | 748 | 748 | 748 |
| mean | 100 | 100 | 100 |
| std | 15.0100 | 15.01 | 15.01 |
| min | 58.9189 | 49.69 | -9.32 |
| 25% | 90.1104 | 89.51 | 90.63 |
| 50% | 99.3473 | 99.78 | 101.09 |
| 75% | 109.6509 | 109.56 | 109.76 |
| max | 144.86 | 140.95 | 138.20 |

**Supplementary Table 2.** Pearson Correlation between the 4 new measures

| | General Control | Flanker Specific | Card Sort Specific | 2-back Specific |
|---|---|---|---|---|
| General Control | -- | -- | -- | -- |
| Flanker Specific | 0.3730*** | -- | -- | -- |
| Card Sort Specific | 0.3671*** | -0.4287*** | -- | -- |
| 2-back Specific | 0.4006*** | -0.1674*** | -0.2422*** | -- |

***: $p<0.001$, uncorrected

**Supplementary Table 3.** Statistics of the new behavior measures

| | General Control | Flanker-specific | Card Sort-specific | 2-Back-specific |
|---|---|---|---|---|
| count | 748 | 748 | 748 | 748 |
| mean | 100 | 100 | 100 | 100 |
| std | 15.010037 | 15.010037 | 15.010037 | 15.010037 |
| min | 50.81347 | 55.554659 | 40.13981 | -17.843425 |
| 25% | 88.847471 | 89.516514 | 90.357072 | 90.915042 |
| 50% | 100.5231 | 99.330337 | 99.688935 | 101.035226 |
| 75% | 110.625526 | 109.315296 | 109.320616 | 110.210396 |
| max | 143.037699 | 156.004711 | 152.515038 | 143.44036 |

**Supplementary Table 4.** CPM prediction accuracy of raw cognitive control measures, volumetric

| | | *Working Memory (2-back)* | | | *Rest* | | |
|---|---|---|---|---|---|---|---|
| | | Flanker | Card Sort | 2-Back | Flanker | Card Sort | 2-Back |
| Positive | Flanker | $0.16^{*,a}$ | $0.13^{\dagger,b}$ | $0.32^{***}$ | $0.15^{***}$ | $0.08^{g}$ | $0.15^{*,h}$ |
| | Card Sort | $0.16^{*,c}$ | $0.21^{***}$ | $0.26^{***}$ | $0.06^{i}$ | $0.15^{*,j}$ | $0.14^{*,k}$ |
| | 2-Back | $0.21^{***}$ | $0.18^{***}$ | $0.37^{***}$ | $0.15^{***}$ | $0.16^{***}$ | $0.20^{***}$ |
| Negative | Flanker | $0.20^{***}$ | $0.13^{\dagger,d}$ | $0.27^{***}$ | $0.10^{l}$ | $0.05^{m}$ | $0.09^{n}$ |
| | Card Sort | $0.16^{*,e}$ | $0.20^{***}$ | $0.25^{***}$ | $0.07^{o}$ | $0.15^{***}$ | $0.19^{***}$ |
| | 2-Back | $0.23^{***}$ | $0.18^{***}$ | $0.35^{***}$ | $0.12^{p}$ | $0.20^{***}$ | $0.22^{***}$ |
| Both | Flanker | $0.20^{***}$ | $0.14^{*,f}$ | $0.31^{***}$ | $0.13^{*,q}$ | $0.07^{r}$ | $0.13^{\dagger,s}$ |
| | Card Sort | $0.18^{***}$ | $0.23^{***}$ | $0.29^{***}$ | $0.07^{t}$ | $0.16^{***}$ | $0.18^{***}$ |
| | 2-Back | $0.25^{***}$ | $0.20^{***}$ | $0.39^{***}$ | $0.15^{*,u}$ | $0.20^{***}$ | $0.23^{***}$ |

$^{***}p<0.001$, $^{**}p<0.01$; $^{*}p<0.05$; $^{\dagger}p<0.1$, all corrected for family-wise error (FWE) after permutation testing. Exact p-values: a: 0.012; b: 0.060; c: 0.024; d: 0.072; e: 0.012; f: 0.012; g: 0.92; h: 0.012; i: 1.76; j: 0.012; k: 0.036; l: 0.22; m: 2.08; n: 0.52; o: 1.48; p: 0.13; q: 0.04; r: 1.20; s: 0.072; t: 1.16; u: 0.024.

**Supplementary Table 5.** t-test statistics for grayordinate vs. volumetric, rest

| | | Flanker | Card Sort | 2-Back |
|---|---|---|---|---|
| Positive | Flanker | -7.92*** | 83.55*** | 62.06*** |
| | Card Sort | 91.19*** | -9.13*** | 128.05*** |
| | 2-Back | 6.78*** | 49.22*** | 38.18*** |
| Negative | Flanker | 40.95*** | 75.49*** | 113.57*** |
| | Card Sort | 25.30*** | -26.16*** | -25.48*** |
| | 2-Back | -6.60*** | -14.74*** | -33.67*** |
| Both | Flanker | 31.19*** | 97.35*** | 111.44*** |
| | Card Sort | 77.78*** | -38.03*** | 66.53*** |
| | 2-Back | 14.25*** | 6.73*** | -1.54*** |

***$p$<0.001. a: p=0.37 (FWE corrected)

**Supplementary Table 6.** CPM prediction accuracy of general and specific control measures, grayordinate, rest

| | | General Control | Flanker Specific | Card Sort Specific | 2-Back Specific |
|---|---|---|---|---|---|
| Positive | General Control | 0.24*** | 0.04 | 0.08 | 0.16*** |
| | Flanker Specific | 0.05 | 0.07 | -0.04 | 0.02 |
| | Card Sort Specific | 0.08 | -0.05 | 0.06 | 0.08 |
| | 2-Back Specific | 0.23*** | 0.05 | 0.08 | 0.16*** |
| Negative | General Control | 0.21*** | 0.01 | 0.09 | 0.14*** |
| | Flanker Specific | 0.02 | 0.11 | -0.07 | -0.02 |
| | Card Sort Specific | 0.06 | -0.04 | 0.06 | 0.05 |
| | 2-Back Specific | 0.20*** | 0.01 | 0.12* | 0.10 |
| Both | General Control | 0.24*** | 0.04 | 0.08 | 0.16*** |
| | Flanker Specific | 0.04 | 0.09 | -0.05 | 0.01 |
| | Card Sort Specific | 0.08 | -0.05 | 0.07 | 0.07 |
| | 2-Back Specific | 0.24*** | 0.03 | 0.10 | 0.15*** |

Each sub-table (bounded by horizontal lines) corresponds to the CPM prediction performance scores using resting-state fMRI and one type of edges (positive, negative, or both). In every 4x4 sub-table, each row represents the training behavior, and each column represents the testing behavior. The maximums of each row and column in the sub-tables are colored in blue and yellow, respectively, with the overlap colored in green. ***$p$<0.001, **p<0.01; *p<0.05; †p<0.1, all corrected for family-wise error (FWE) after permutation testing.

**Supplementary Table 7.** CPM prediction accuracy of general and specific control measures, volumetric, 2-back

| | | General Control | Flanker Specific | Card Sort Specific | 2-Back Specific |
|---|---|---|---|---|---|
| Positive | General Control | 0.32*** | 0.08 | 0.02 | 0.29*** |
| | Flanker Specific | 0.09 | 0.06 | -0.07 | 0.12 |
| | Card Sort Specific | 0.06 | -0.04 | 0.11 | -0.01 |
| | 2-Back Specific | 0.32*** | 0.10 | 0.00 | 0.30*** |
| Negative | General Control | 0.32*** | 0.09 | 0.03 | 0.26*** |
| | Flanker Specific | 0.14† | 0.10 | -0.05 | 0.13 |
| | Card Sort Specific | 0.03 | -0.04 | 0.07 | -0.01 |
| | 2-Back Specific | 0.29*** | 0.10 | -0.01 | 0.26*** |
| Both | General Control | 0.35*** | 0.09 | 0.03 | 0.29*** |
| | Flanker Specific | 0.13 | 0.09 | -0.07 | 0.14† |
| | Card Sort Specific | 0.05 | -0.04 | 0.10 | -0.01 |
| | 2-Back Specific | 0.33*** | 0.11 | -0.01 | 0.30*** |

Each sub-table (bounded by horizontal lines) corresponds to the CPM prediction performance scores using 2-back task-fMRI and one type of edges (positive, negative, or both). In every 4x4 sub-table, each row represents the training behavior, and each column represents the testing behavior. The maximums of each row and column in the sub-tables are colored in blue and yellow, respectively, with the overlap colored in green. ***$p$<0.001, **p<0.01; *p<0.05; †p<0.1, all corrected for family-wise error (FWE) after permutation testing.

**Supplementary Table 8.** CPM prediction accuracy of general and specific control measures, volumetric, rest

| | | General Control | Flanker Specific | Card Sort Specific | 2-Back Specific |
|---|---|---|---|---|---|
| Positive | General Control | 0.23*** | 0.07 | 0.03 | 0.16*** |
| | Flanker Specific | 0.09 | 0.10 | -0.05 | 0.06 |
| | Card Sort Specific | 0.04 | -0.07 | 0.12† | 0.00 |
| | 2-Back Specific | 0.17* | 0.04 | 0.05 | 0.11 |
| Negative | General Control | 0.22*** | -0.01 | 0.10 | 0.18*** |
| | Flanker Specific | 0.01 | 0.08 | -0.07 | 0.00 |
| | Card Sort Specific | 0.06 | -0.06 | 0.08 | 0.04 |
| | 2-Back Specific | 0.17*** | -0.01 | 0.09 | 0.12† |
| Both | General Control | 0.25*** | 0.04 | 0.07 | 0.19*** |
| | Flanker Specific | 0.07 | 0.10 | -0.06 | 0.04 |
| | Card Sort Specific | 0.06 | -0.06 | 0.09 | 0.04 |
| | 2-Back Specific | 0.18*** | 0.01 | 0.08 | 0.13* |

Each sub-table (bounded by horizontal lines) corresponds to the CPM prediction performance scores using resting-state fMRI and one type of edges (positive, negative, or both). In every 4x4 sub-table, each row represents the training behavior, and each column represents the testing behavior. The maximums of each row and column in the sub-tables are colored in blue and yellow, respectively, with the overlap colored in green. ***$p$<0.001, **p<0.01; *p<0.05; †p<0.1, all corrected for family-wise error (FWE) after permutation testing.

**Supplementary Table 9a.** Use general attention CPM to predict the general and specific control measures, volumetric, rest, both edges

| | General Control | Flanker Specific | Card Sort Specific | 2-back Specific |
|---|---|---|---|---|
| General Attention CPM | 0.11$^{*, a}$ | 0.06 | 0.08 | 0.05 |
| General Control CPM | 0.25$^{***}$ | 0.04 | 0.07 | 0.19$^{***}$ |

The general attention CPM cross-prediction performance is calculated by correlating the predicted behavior measure with the actual behavior measure. The general control CPM results are from Table 9. The p-values are corrected by FWE. $^{***}$p<0.001, $^{**}$p<0.01, $^{*}$p<0.05; $^{\dagger}$p<0.1. p-values: a: 0.031.

**Supplementary 9b.** Use general attention CPM to predict the original control measures, volumetric, rest, both edges

| | Flanker | Card Sort | 2-back |
|---|---|---|---|
| General Attention CPM | 0.08 | 0.11$^{*, a}$ | 0.09 |
| General Control CPM | 0.15$^{**, b}$ | 0.18$^{***}$ | 0.25$^{***}$ |

The model performance is calculated by correlating the predicted behavior measure (by the general attention CPM) with the actual behavior measure. The general control CPM results are obtained via the regular CPM train/test procedure. The p-values are corrected by FWE. $^{***}$p<0.001, $^{**}$p<0.01, $^{*}$p<0.05; $^{\dagger}$p<0.1. p-values: a: 0.031, b: 0.006.

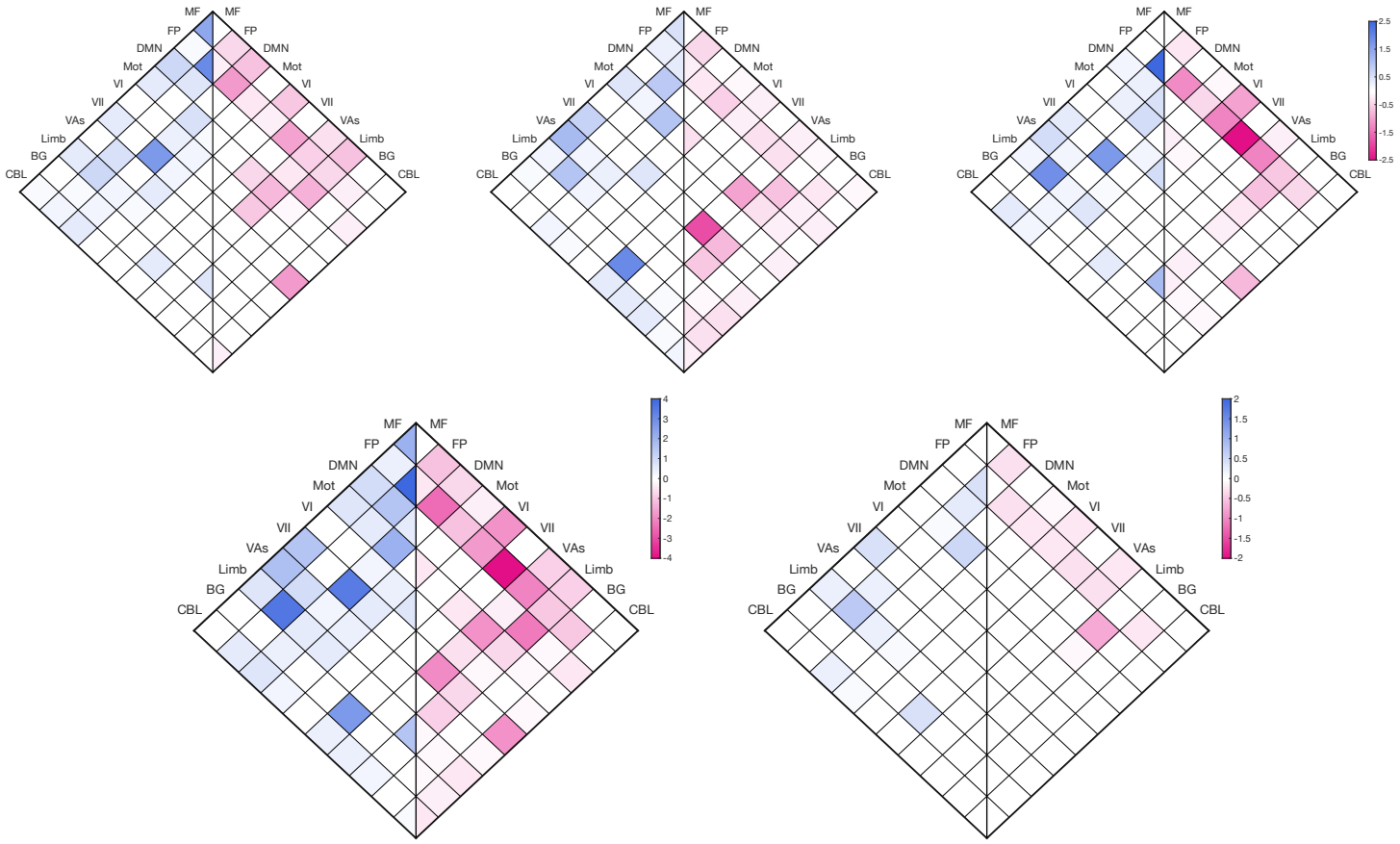


Positive Network | Negative Network

**Supplementary Figure 1.** CPM Canonical network analysis, using 2-Back, volumetric fMRI
Top 3: Flanker, Card Sort, 2-back; Bottom 2: Union, Intersection
Network Acronyms: MF, medial frontal; FP, frontoparietal; DMN, default-mode; Mot, motor; VI, visual A; VII, visual B; VAs, visual association; Limb, limbic; BG, basal ganglia; CBL, cerebellum

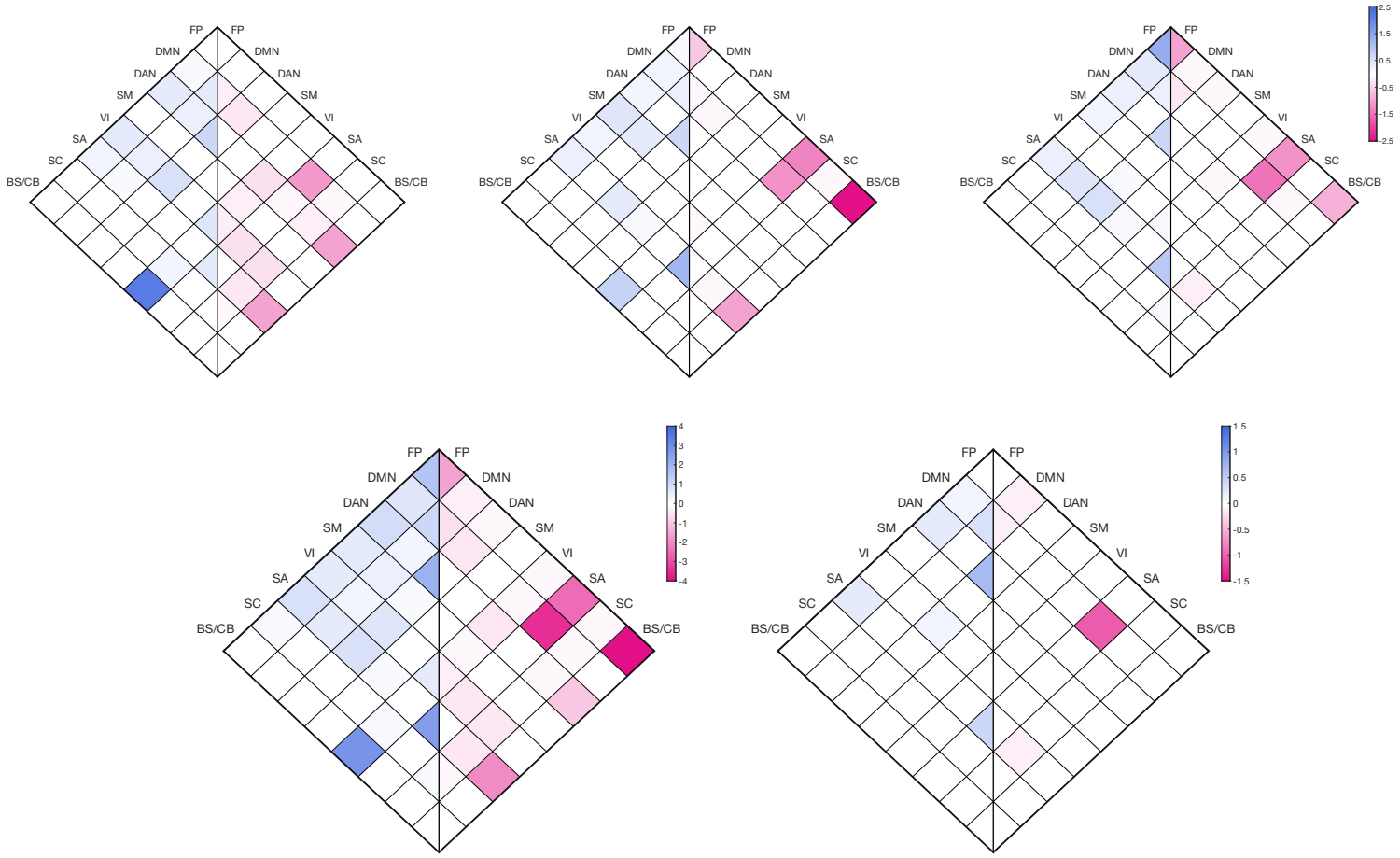


Positive Network | Negative Network

**Supplementary Figure 2.** CPM Canonical network analysis, using resting, grayordinate fMRI

Top 3: Flanker, Card Sort, 2-back; Bottom 2: Union, Intersection

Network Acronyms: FP, frontoparietal; DM, default mode; DA, dorsal attention; SM, somatomotor; VI, visual; SA, salience; SC, subcortical; BS/CB, brain stem/cerebellum.

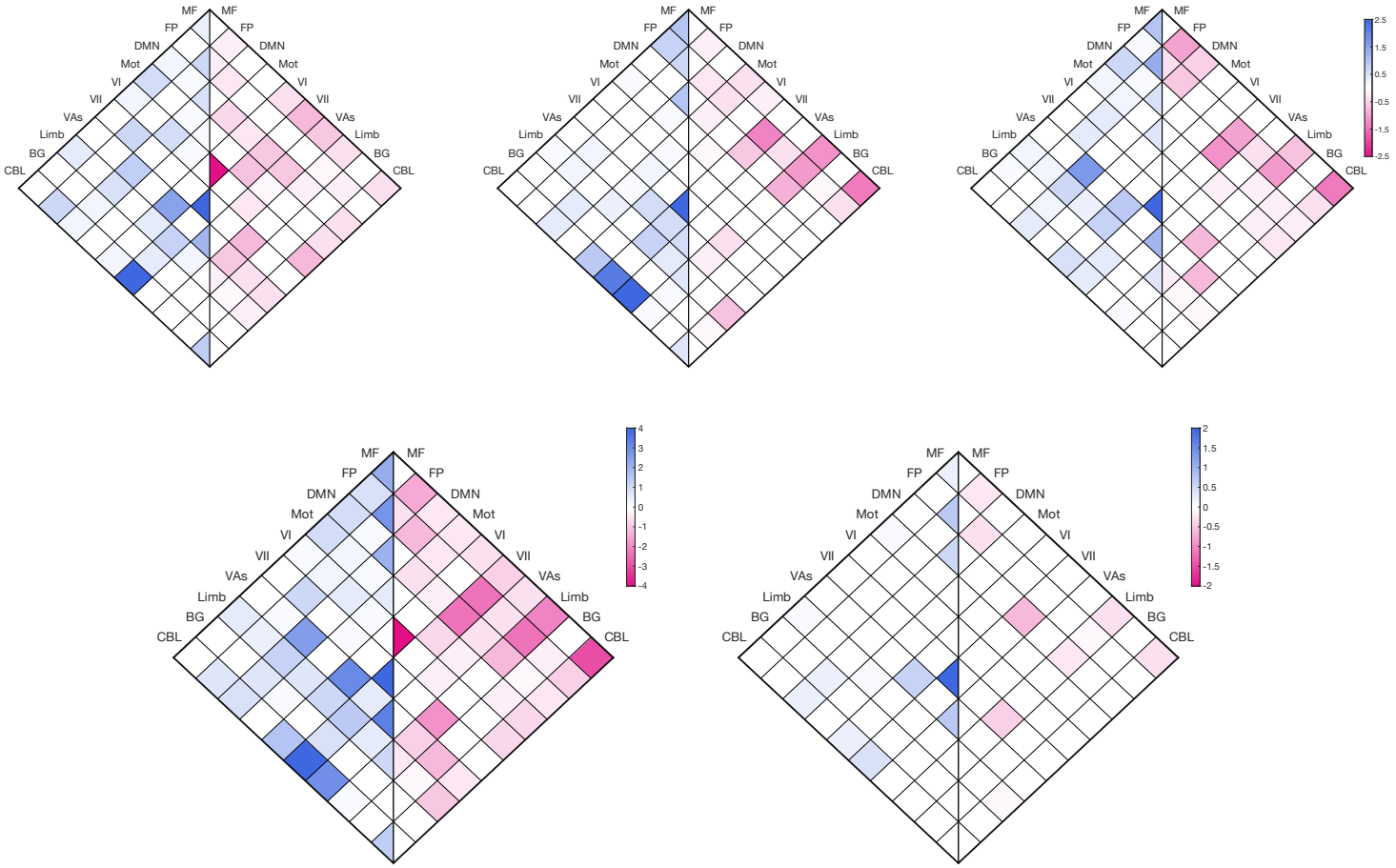


Positive Network | Negative Network

**Supplementary Figure 3.** CPM Canonical network analysis, using resting, volumetric fMRI
Top 3: Flanker, Card Sort, 2-back; Bottom 2: Union, Intersection
Network Acronyms: MF, medial frontal; FP, frontoparietal; DMN, default-mode; Mot, motor; VI, visual A; VII, visual B; VAs, visual association; Limb, limbic; BG, basal ganglia; CBL, cerebellum

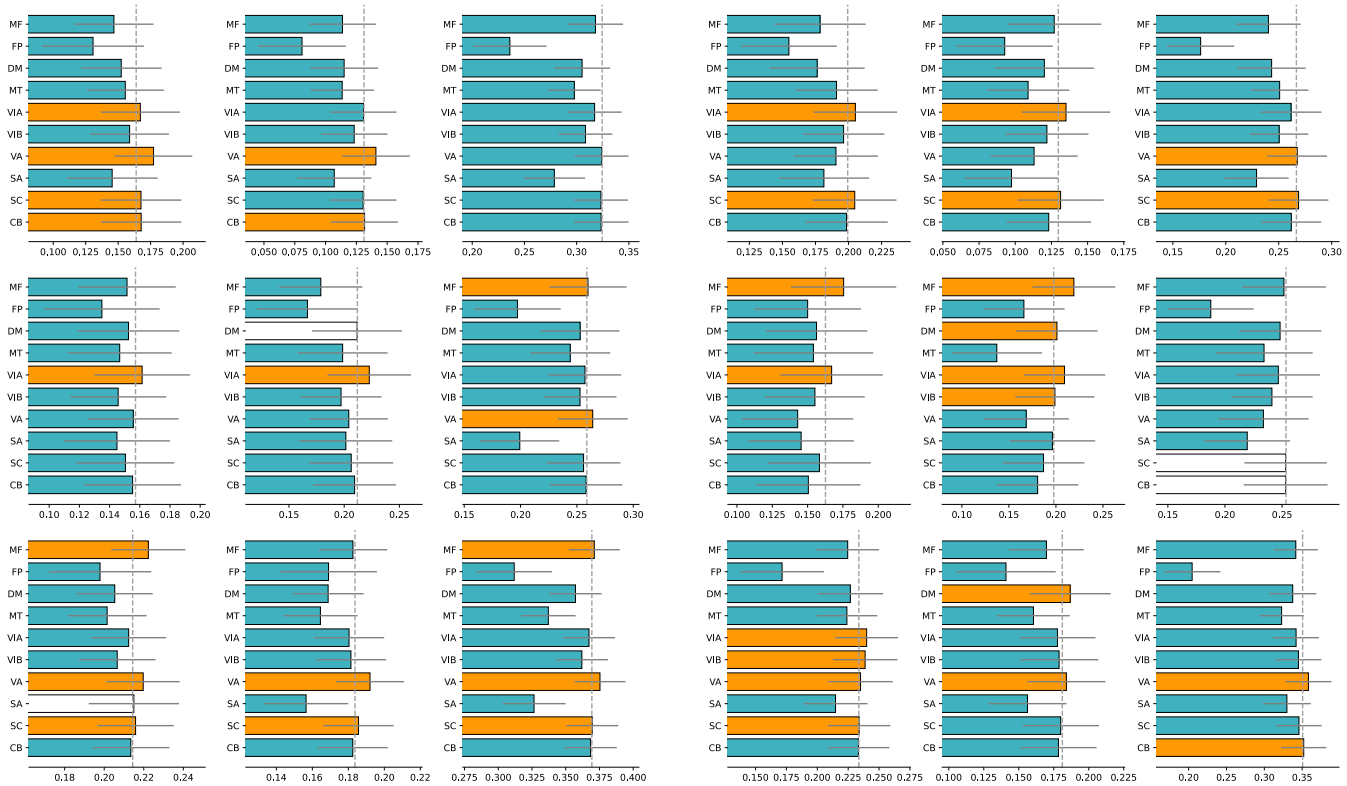


**Supplementary Figure 4.** CPM lesion analysis on 2-Back, volumetric fMRI data.

Left: lesioning positive edge; Right: lesioning negative edges; Rows are training behaviors, in order of: Flanker, Card Sort, 2-back. Columns are testing behaviors, in the same order as rows. Colorings and notations all follow **Figure 2** in the main article. Besides those listed below, all the p-values are < 0.001 after FWE correction.

Exact p-values:

listed in format of (training task-testing task, network name, type of edge, corrected p value)

Flanker-2Back, VA, positive, p=0.007; Card Sort-Card Sort, DM, positive, p=39.91; Card Sort-2Back, MF, positive, p=0.005; 2Back-Flanker, SA, positive, p=0.077; Flanker-2Back, VA, negative, p=0.048; Card Sort-2Back, SC, negative, p=2.89; Card Sort-2Back, CB, negative, p=1.34; 2Back-Flanker, SC, negative, p=0.027;

**Supplementary Figure 5.** CPM lesion analysis on resting, grayordinate fMRI data.

Left: lesioning positive edge; Right: lesioning negative edges; Rows are training behaviors, in order of: Flanker, Card Sort, 2-back. Columns are testing behaviors, in the same order as rows. Colorings and notations all follow **Figure 2** in the main article. Besides those listed below, all the p-values are < 0.001 after FWE correction.

Exact p-values:

listed in format of (training task-testing task, network name, type of edge, corrected p value)

Flanker-Card Sort, SC, positive, p=30.34; Flanker-2Back, SM, positive, p=0.020; Card Sort-Flanker, DM, positive, p=0.029; Card Sort-Flanker, DA, positive, p=36.70; Card Sort-2Back, BS/CB, positive, p=0.317; 2Back-Flanker, VI, positive, p=58.67; 2-Back-Flanker, BS/CB, positive, p=Nan; 2Back-Card Sort, BS/CB, positive, p=NaN; 2Back-2Back, BS/CB, positive, p=NaN; Flanker-2Back, FP, negative, p=0.13; Flanker-2Back, VI, negative, p=10.94; 2Back-Card Sort, SM, negative, p=18.53;

**Supplementary Figure 6.** CPM lesion analysis on resting, volumetric fMRI data. Left: lesioning positive edge; Right: lesioning negative edges; Rows are training behaviors, in order of: Flanker, Card Sort, 2-back. Columns are testing behaviors, in the same order as rows. Colorings and notations all follow **Figure 2** in the main article. Besides those listed below, all the p-values are < 0.001 after FWE correction.

Exact p-values:
listed in format of (training task-testing task, network name, type of edge, corrected p value)
Flanker-2Back, SC, positive, p=13.87; Card Sort-Flanker, CB, positive, p=0.001; Card Sort-Card Sort, VIB, positive, p=49.90; 2-Back-Flanker, MF, positive, p=27.30; Flanker-Card Sort, VIA, negative, p=0.94; Card Sort-Flanker, CB, negative, p=0.18; Card Sort-Card Sort, VIB, negative, p=13.07; 2Back-2Back, SC, negative, p=0.53.

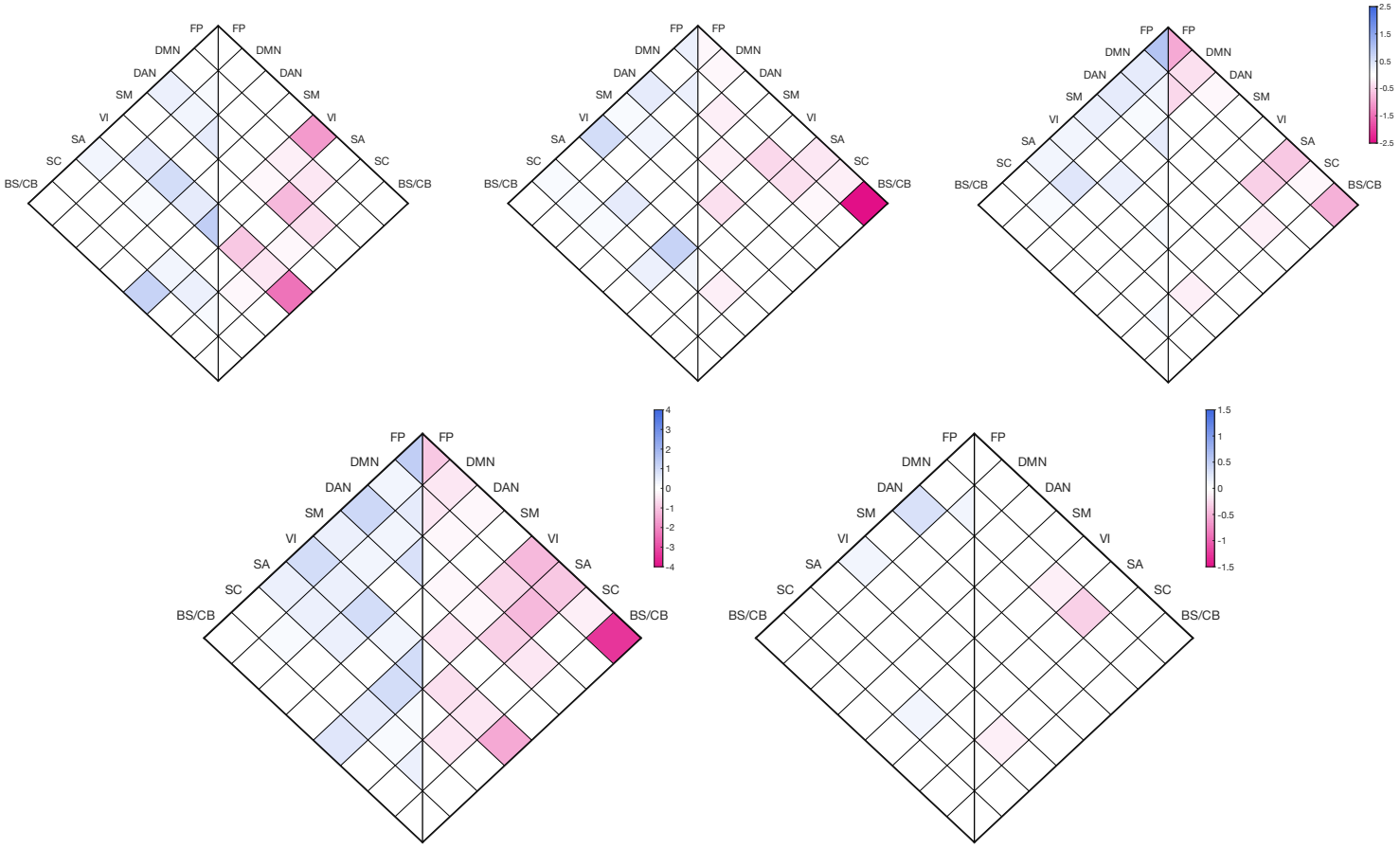


Positive Network | Negative Network

**Supplementary Figure 7.** CPM canonical network analysis of component-specific measures using resting-state, Grayordinate fMRI data.
Top 3: Flanker-specific, Card Sort-specific, 2-back-specific; Bottom 2: Union, Intersection
Network Acronyms: FP, frontoparietal; DM, default mode; DA, dorsal attention; SM, somatomotor; VI, visual; SA, salience; SC, subcortical; BS/CB, brain stem/cerebellum.

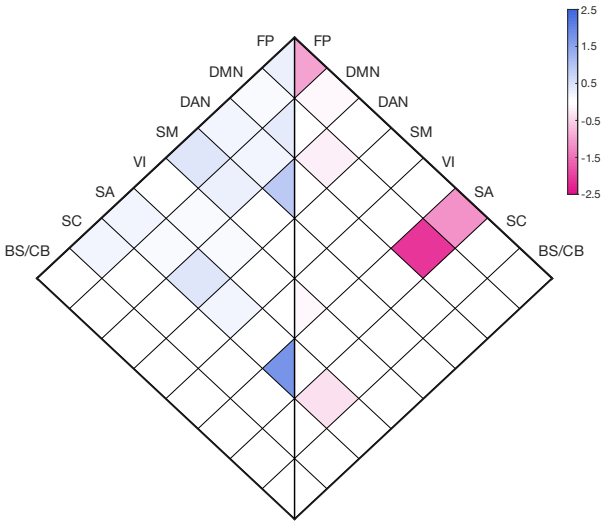


Positive Network | Negative Network

**Supplementary Figure 8.** CPM canonical network analysis of general control using resting-state, Grayordinate fMRI data.

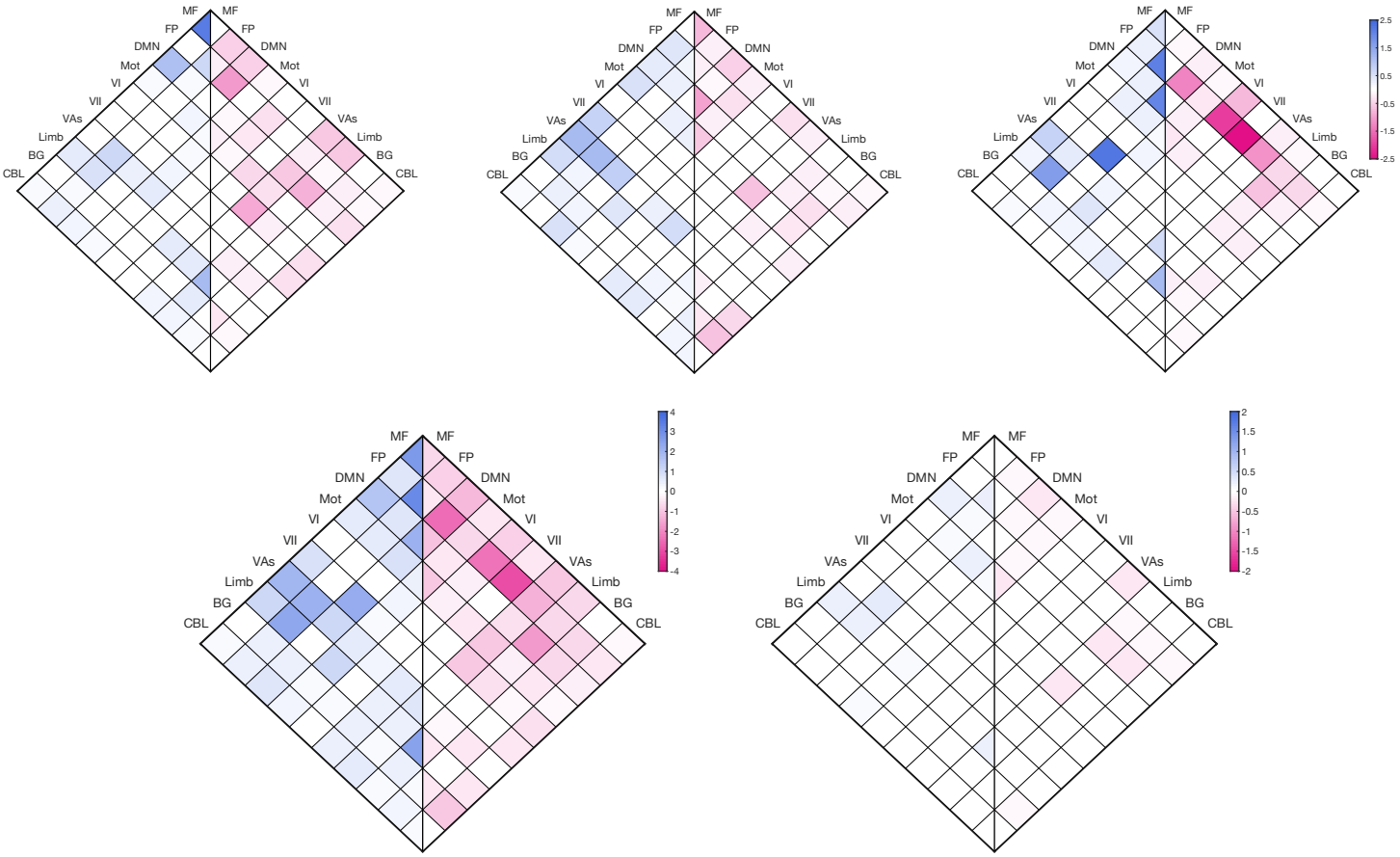


Positive Network | Negative Network

**Supplementary Figure 9.** CPM canonical network analysis of component-specific measures using 2-back, volumetric fMRI data.
Top 3: Flanker-specific, Card Sort-specific, 2-back-specific; Bottom 2: Union, Intersection
Network acronyms: MF, medial frontal; FP, frontoparietal; DMN, default-mode; Mot, motor; VI, visual A; VII, visual B; VAs, visual association; Limb, limbic; BG, basal ganglia; CBL, cerebellum

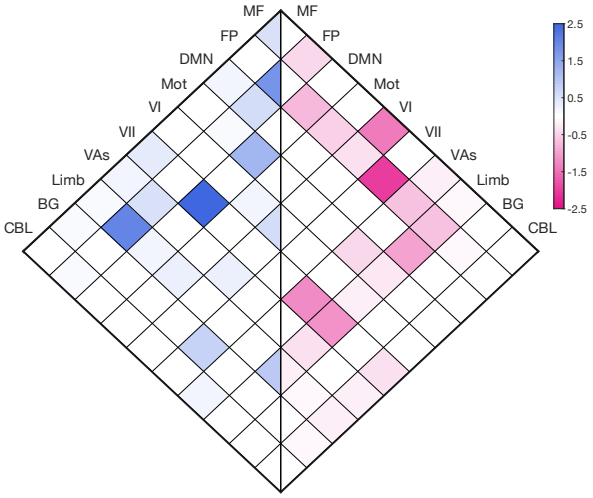


Positive Network | Negative Network

**Supplementary Figure 10.** CPM canonical network analysis of general control using 2-back, volumetric fMRI data.

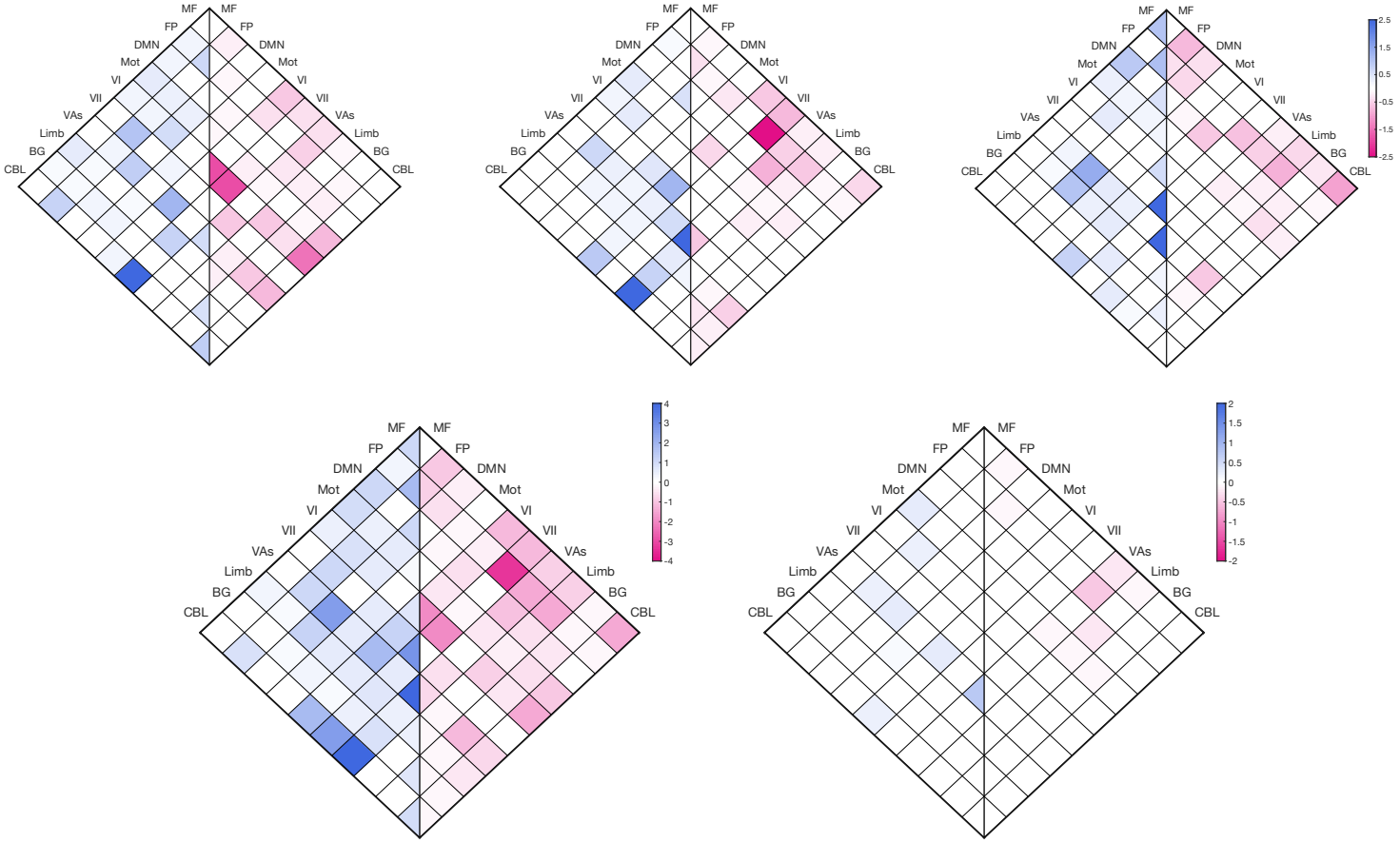


Positive Network | Negative Network

**Supplementary Figure 11.** CPM canonical network analysis of component-specific measures using resting, volumetric fMRI data.
Top 3: Flanker-specific, Card Sort-specific, 2-back-specific; Bottom 2: Union, Intersection
Network acronyms: MF, medial frontal; FP, frontoparietal; DMN, default-mode; Mot, motor; VI, visual A; VII, visual B; VAs, visual association; Limb, limbic; BG, basal ganglia; CBL, cerebellum

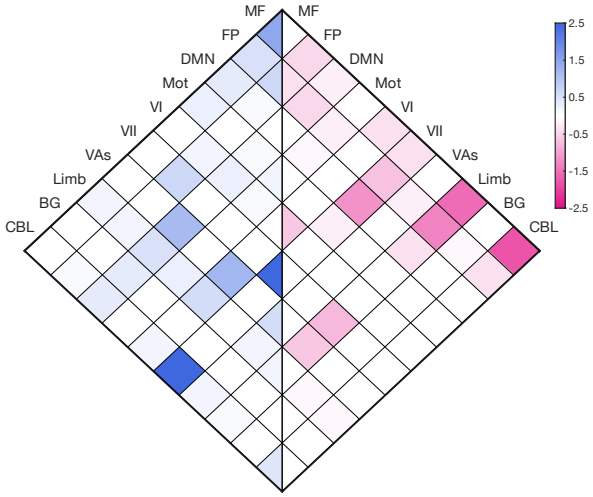


Positive Network | Negative Network

**Supplementary Figure 12.** CPM canonical network analysis of general control using resting, volumetric fMRI data.